Gebe, J.A., Kiener, P.A., Ring, H.Z., Li, X., Francke, U., and Aruffo, A. (1997). Molecular cloning, mapping to human chromosome 1 q21-q23, and cell binding characteristics of Spalpha, a new member of the scavenger receptor cysteine-rich (SRCR) family of proteins. J. Biol. Chem. *272*, 6151–6158.

Gebe, J.A., Llewellyn, M., Hoggatt, H., and Aruffo, A. (2000). Molecular cloning, genomic organization and cell-binding characteristics of mouse Spalpha. Immunology *99*, 78–86.

Giodini, A., and Cresswell, P. (2008). Hsp90-mediated cytosolic refolding of exogenous proteins internalized by dendritic cells. EMBO J. *27*, 201–211.

Gray, J., Chattopadhyay, D., Beale, G.S., Patman, G.L., Miele, L., King, B.P., Stewart, S., Hudson, M., Day, C.P., Manas, D.M., and Reeves, H.L. (2009). A proteomic strategy to identify novel serum biomarkers for liver cirrhosis and hepatocellular cancer in individuals with fatty liver disease. BMC Cancer *9*, 271.

Greenwalt, D.E., Lipsky, R.H., Ockenhouse, C.F., Ikeda, H., Tandon, N.N., and Jamieson, G.A. (1992). Membrane glycoprotein CD36: a review of its roles in adherence, signal transduction, and transfusion medicine. Blood *80*, 1105–1115.

Haug, G., Leemhuis, J., Tiemann, D., Meyer, D.K., Aktories, K., and Barth, H. (2003). The host cell chaperone Hsp90 is essential for translocation of the binary Clostridium botulinum C2 toxin into the cytosol. J. Biol. Chem. *278*, 32266–32274.

He, W., Barak, Y., Hevener, A., Olson, P., Liao, D., Le, J., Nelson, M., Ong, E., Olefsky, J.M., and Evans, R.M. (2003). Adipose-specific peroxisome proliferator-activated receptor gamma knockout causes insulin resistance in fat and liver but not in muscle. Proc. Natl. Acad. Sci. USA *100*, 15712–15717.

Holm, C. (2003). Molecular mechanisms regulating hormone-sensitive lipase and lipolysis. Biochem. Soc. Trans. *31*, 1120–1124.

Ibrahimi, A., and Abumrad, N.A. (2002). Role of CD36 in membrane transport of long-chain fatty acids. Curr. Opin. Clin. Nutr. Metab. Care *5*, 139–145.

Joseph, S.B., Bradley, M.N., Castrillo, A., Bruhn, K.W., Mak, P.A., Pei, L., Hogenesch, J., O'connell, R.M., Cheng, G., Saez, E., et al. (2004). LXR-dependent gene expression is important for macrophage survival and the innate immune response. Cell *119*, 299–309.

Kelley, D.S., Nelson, G.J., and Hunt, J.E. (1986). Effect of prior nutritional status on the activity of lipogenic enzymes in primary monolayer cultures of rat hepatocytes. Biochem. J. *235*, 87–90.

Kim, W.K., Hwang, H.R., Kim, H., Lee, P.Y., In, Y.J., Ryu, H.Y., Park, S.G., Bae, K.H., and Lee, S.C. (2008). Glycoproteomic analysis of plasma from patients with atopic dermatitis: CD5L and ApoE as potential biomarkers. Exp. Mol. Med. *40*, 677–685.

Kovacs, P., Harper, I., Hanson, R.L., Infante, A.M., Bogardus, C., Tataranni, P.A., and Baier, L.J. (2004). A novel missense substitution (Val1483Ile) in the fatty acid synthase gene (FAS) is associated with percentage of body fat and substrate oxidation rates in nondiabetic Pima Indians. Diabetes *53*, 1915–1919.

Kuhajda, F.P., Pizer, E.S., Li, J.N., Mani, N.S., Frehywot, G.L., and Townsend, C.A. (2000). Synthesis and antitumor activity of an inhibitor of fatty acid synthase. Proc. Natl. Acad. Sci. USA *97*, 3450–3454.

Kumar, M.V., Shimokawa, T., Nagy, T.R., and Lane, M.D. (2002). Differential effects of a centrally acting fatty acid synthase inhibitor in lean and obese mice. Proc. Natl. Acad. Sci. USA *99*, 1921–1925.

Kuwata, K., Watanabe, H., Jiang, S.Y., Yamamoto, T., Tomiyama-Miyaji, C., Abo, T., Miyazaki, T., and Naito, M. (2003). AIM inhibits apoptosis of T cells and NKT cells in Corynebacterium-induced granuloma formation in mice. Am. J. Pathol. *162*, 837–847.

Lafontan, M. (2008). Advances in adipose tissue metabolism. Int. J Obes. (Lond) *32* (*Suppl 7*), S39–S51.

Lin, S.Y., Makino, K., Xia, W., Matin, A., Wen, Y., Kwong, K.Y., Bourguignon, L., and Hung, M.C. (2001). Nuclear localization of EGF receptor and its potential new role as a transcription factor. Nat. Cell Biol. *3*, 802–808.

Liu, L.H., Wang, X.K., Hu, Y.D., Kang, J.L., Wang, L.L., and Li, S. (2004). Effects of a fatty acid synthase inhibitor on adipocyte differentiation of mouse 3T3-L1 cells. Acta Pharmacol. Sin. *25*, 1052–1057.

Loftus, T.M., Jaworsky, D.E., Frehywot, G.L., Townsend, C.A., Ronnett, G.V., Lane, M.D., and Kuhajda, F.P. (2000). Reduced food intake and body weight in mice treated with fatty acid synthase inhibitors. Science *288*, 2379–2381.

Lupu, R., and Menendez, J.A. (2006). Pharmacological inhibitors of Fatty Acid Synthase (FASN)—catalyzed endogenous fatty acid biogenesis: a new family of anti-cancer agents? Curr. Pharm. Biotechnol. *7*, 483–493.

Madsen, L., Petersen, R.K., Sørensen, M.B., Jørgensen, C., Hallenborg, P., Pridal, L., Fleckner, J., Amri, E.Z., Krieg, P., Furstenberger, G., et al. (2003). Adipocyte differentiation of 3T3-L1 preadipocytes is dependent on lipoxygenase activity during the initial stages of the differentiation process. Biochem. J. *375*, 539–549.

Makimura, H., Mizuno, T.M., Yang, X.J., Silverstein, J., Beasley, J., and Mobbs, C.V. (2001). Cerulenin mimics effects of leptin on metabolic rate, food intake, and body weight independent of the melanocortin system, but unlike leptin, cerulenin fails to block neuroendocrine effects of fasting. Diabetes *50*, 733–739.

Menendez, J.A., and Lupu, R. (2007). Fatty acid synthase and the lipogenic phenotype in cancer pathogenesis. Nat. Rev. Cancer *7*, 763–777.

Miyazaki, T., Hirokami, Y., Matsuhashi, N., Takatsuka, H., and Naito, M. (1999). Increased susceptibility of thymocytes to apoptosis in mice lacking AIM, a novel murine macrophage-derived soluble factor belonging to the scavenger receptor cysteine-rich domain superfamily. J. Exp. Med. *189*, 413–422.

Mobbs, C.V., and Makimura, H. (2002). Block the FAS, lose the fat. Nat. Med. *8*, 335–336.

Neels, J.G., and Olefsky, J.M. (2006). Inflamed fat: what starts the fire? J. Clin. Invest. *116*, 33–35.

Nishino, N., Tamori, Y., Tateya, S., Kawaguchi, T., Shibakusa, T., Mizunoya, W., Inoue, K., Kitazawa, R., Kitazawa, S., Matsuki, Y., et al. (2008). FSP27 contributes to efficient energy storage in murine white adipocytes by promoting the formation of unilocular lipid droplets. J. Clin. Invest. *118*, 2808–2821.

Olshansky, S.J., Passaro, D.J., Hershow, R.C., Layden, J., Carnes, B.A., Brody, J., Hayflick, L., Butler, R.N., Allison, D.B., and Ludwig, D.S. (2005). A potential decline in life expectancy in the United States in the 21st century. N. Engl. J. Med. *352*, 1138–1145.

Olsnes, S., Klingenberg, O., and Wiedłocha, A. (2003). Transport of exogenous growth factors and cytokines to the cytosol and to the nucleus. Physiol. Rev. *83*, 163–182.

Puri, V., and Czech, M.P. (2008). Lipid droplets: FSP27 knockout enhances their sizzle. J. Clin. Invest. *118*, 2693–2696.

Qu, P., Du, H., Li, Y., and Yan, C. (2009). Myeloid-specific expression of Api6/AIM/Sp alpha induces systemic inflammation and adenocarcinoma in the lung. J. Immunol. *182*, 1648–1659.

Ratts, R., Zeng, H., Berg, E.A., Blue, C., McComb, M.E., Costello, C.E., vanderSpek, J.C., and Murphy, J.R. (2003). The cytosolic entry of diphtheria toxin catalytic domain requires a host cell cytosolic translocation factor complex. J. Cell Biol. *160*, 1139–1150.

Ronnett, G.V., Kim, E.K., Landree, L.E., and Tu, Y. (2005). Fatty acid metabolism as a target for obesity treatment. Physiol. Behav. *85*, 25–35.

Rosen, E.D., Sarraf, P., Troy, A.E., Bradwin, G., Moore, K., Milstone, D.S., Spiegelman, B.M., and Mortensen, R.M. (1999). PPAR gamma is required for the differentiation of adipose tissue in vivo and in vitro. Mol. Cell *4*, 611–617.

Sandvig, K., and van Deurs, B. (2000). Entry of ricin and Shiga toxin into cells: molecular mechanisms and medical perspectives. EMBO J. *19*, 5943–5950.

Sandvig, K., and van Deurs, B. (2005). Delivery into cells: lessons learned from plant and bacterial toxins. Gene Ther. *12*, 865–872.

Schmid, B., Rippmann, J.F., Tadayyon, M., and Hamilton, B.S. (2005). Inhibition of fatty acid synthase prevents preadipocyte differentiation. Biochem. Biophys. Res. Commun. *328*, 1073–1082.

Shimokawa, T., Kumar, M.V., and Lane, M.D. (2002). Effect of a fatty acid synthase inhibitor on food intake and expression of hypothalamic neuropeptides. Proc. Natl. Acad. Sci. USA *99*, 66–71.

Shoelson, S.E., Lee, J., and Goldfine, A.B. (2006). Inflammation and insulin resistance. J. Clin. Invest. *116*, 1793–1801.

Smas, C.M., and Sul, H.S. (1993). Pref-1, a protein containing EGF-like repeats, inhibits adipocyte differentiation. Cell *73*, 725–734.

Smith, S. (1994). The animal fatty acid synthase: one gene, one polypeptide, seven enzymes. FASEB J. *8*, 1248–1259.

Smith, S., Stern, A., Randhawa, Z.I., and Knudsen, J. (1985). Mammalian fatty acid synthetase is a structurally and functionally symmetrical dimer. Eur. J. Biochem. *152*, 547–555.

Surmi, B.K., and Hasty, A.H. (2008). Macrophage infiltration into adipose tissue: initiation, propagation and remodeling. Future Lipidol. *3*, 545–556.

Valledor, A.F., Hsu, L.C., Ogawa, S., Sawka-Verhelle, D., Karin, M., and Glass, C.K. (2004). Activation of liver X receptors and retinoid X receptors prevents bacterial-induced macrophage apoptosis. Proc. Natl. Acad. Sci. USA *101*, 17813–17818.

Wesche, J., Małecki, J., Wiedłocha, A., Skjerpen, C.S., Claus, P., and Olsnes, S. (2006). FGF-1 and FGF-2 require the cytosolic chaperone Hsp90 for translocation into the cytosol and the cell nucleus. J. Biol. Chem. *281*, 11405–11412.

Wu, Z., Puigserver, P., and Spiegelman, B.M. (1999a). Transcriptional activation of adipogenesis. Curr. Opin. Cell Biol. *11*, 689–694.

Wu, Z., Rosen, E.D., Brun, R., Hauser, S., Adelmant, G., Troy, A.E., McKeon, C., Darlington, G.J., and Spiegelman, B.M. (1999b). Cross-regulation of C/EBP alpha and PPAR gamma controls the transcriptional pathway of adipogenesis and insulin sensitivity. Mol. Cell *3*, 151–158.

Yusa, S., Ohnishi, S., Onodera, T., and Miyazaki, T. (1999). AIM, a murine apoptosis inhibitory factor, induces strong and sustained growth inhibition of B lymphocytes in combination with TGF-β1. Eur. J. Immunol. *29*, 1086–1093.

Zechner, R., Strauss, J.G., Haemmerle, G., Lass, A., and Zimmermann, R. (2005). Lipolysis: pathway under construction. Curr. Opin. Lipidol. *16*, 333–340.

Biochemical and Biophysical Research Communications 391 (2010) 1708–1713

Contents lists available at ScienceDirect

Biochemical and Biophysical Research Communications

journal homepage: www.elsevier.com/locate/ybbrc

The death effector domain-containing DEDD forms a complex with Akt and Hsp90, and supports their stability

Nobuya Kurabe [1], Mayumi Mori, Jun Kurokawa, Kaori Taniguchi, Hisatoshi Aoyama, Kazuhiro Atsuda, Akemi Nishijima, Nariaki Odawara, Saori Harada, Katsuhiko Nakashima, Satoko Arai, Toru Miyazaki *

Division of Molecular Biomedicine for Pathogenesis, Center for Disease Biology and Integrative Medicine, Faculty of Medicine, The University of Tokyo, 7-3-1, Hongo, Bunkyo-ku, Tokyo 113-0033, Japan

ARTICLE INFO

Article history:
Received 22 December 2009
Available online 30 December 2009

Keywords:
DEDD
Akt
Glucose uptake
Cdk1

ABSTRACT

Insulin secretion and glucose transport are the major mechanisms to balance glucose homeostasis. Recently, we found that the death effector domain-containing DEDD inhibits cyclin-dependent kinase-1 (Cdk1) function, thereby preventing Cdk1-dependent inhibitory phosphorylation of S6 kinase-1 (S6K1), downstream of phosphatidylinositol 3-kinase (PI3K), which overall results in maintenance of S6K1 activity. Here we newly show that DEDD forms a complex with Akt and heat-shock protein 90 (Hsp90), and supports the stability of both proteins. Hence, in DEDD$^{-/-}$ mice, Akt protein levels are diminished in skeletal muscles and adipose tissues, which interferes with the translocation of glucose-transporter 4 (GLUT4) upon insulin stimulation, leading to inefficient incorporation of glucose in these organs. Interestingly, as for the activation of S6K1, suppression of Cdk1 is involved in the stabilization of Akt protein by DEDD, since diminishment of Cdk1 in DEDD$^{-/-}$ cells via siRNA expression or treatment with a Cdk1-inhibitor, increases both Akt and Hsp90 protein levels. Such multifaceted involvement of DEDD in glucose homeostasis by supporting both insulin secretion (via maintenance of S6K1 activity) and glucose uptake (via stabilizing Akt protein), may suggest an association of DEDD-deficiency with the pathogenesis of type 2 diabetes mellitus.

Introduction

The signalling cascade involving mitogen-related phosphatidylinositol 3-kinase (PI3K), Akt and their downstream TOR (target of rapamycin) is the central pathway that maintains glucose homeostasis in the body [1–4]. In mammals, upon stimulation by growth factors including insulin, the mammalian TOR (mTOR) cooperates with PI3K-dependent effectors to activate p70 ribosomal protein S6 kinase-1 (S6K1), thereby phosphorylating the 40S-ribosomal protein S6, and subsequently enhances translation of the 5′-terminal oligopyrimidine (5′-TOP) sequences that encode components of the translational machinery. This reaction increases the number of ribosomes and the efficacy of protein synthesis, thus critically promoting growth of types of cells including insulin-producing β cells within the pancreatic Langerhans islet [5–8]. The insulin mass was diminished in S6K1-deficient (S6K1$^{-/-}$) mice, resulting in ineffective secretion of insulin upon glucose administration [9]. Thus, S6K1 is involved in the machinery controlling glucose tolerance by supporting the size of β cells [10,11]. On the other hand, activation of Akt (in particular Akt2, the primary isoform in insulin-responsive tissues) induces translocation of glucose-transporter 4 (GLUT4) to the plasma membrane [12–15]. This response is responsible for glucose transport into cells. Thus, dysfunction of these elements provokes a phenotype similar to type 2 diabetes mellitus, which is a multifactorial disease with a variety of pathological defects in glucose homeostasis [16–18].

Recently, we defined the DEDD molecule as a critical element that maintains the activity of S6K1, thereby supporting the size of β cells and insulin mass in mice [19]. DEDD was initially described as a member of the death effector domain (DED)-containing protein family [20]. We previously found that DEDD is associated with the Cdk1/cyclin B1 complex, and that it decreases the kinase activity of Cdk1 [21]. This response impedes the Cdk1-dependent mitotic program to shut off synthesis of ribosomal RNA (rRNA) and protein, and is consequently useful in gaining sufficient cell growth [21,22]. Interestingly, DEDD also associates with S6K1, and interferes with the Cdk1-dependent inhibitory phosphorylation of S6K1 at several serine/threonine (Ser/Thr)

Abbreviations: DEDD, death effector domain-containing DNA binding protein; Cdk1, cyclin-dependent kinase-1; S6K1, S6 kinase-1; PI3K, phosphatidylinositol 3-kinase; rRNA, ribosomal RNA; TOR, target of rapamycin; mTOR, mammalian TOR; 5′-TOP, 5′-terminal oligopyrimidine; Thr, threonine; Ser, serine; MEF, mouse embryonic fibroblast; PDK1, phosphoinositide-dependent protein kinase-1; Hsp90, heat-shock protein 90; GLUT4, glucose-transporter 4.

* Corresponding author. Fax: +81 3 5841 1438.
E-mail address: tm@m.u-tokyo.ac.jp (T. Miyazaki).
[1] Present address: Department of Molecular Anatomy, Hamamatsu University School of Medicine, Hamamatsu, Shizuoka 431-3192, Japan.

0006-291X/$ - see front matter © 2009 Elsevier Inc. All rights reserved.
doi:10.1016/j.bbrc.2009.12.137

residues, including Ser411 and Ser424 sites within the auto-inhibitory tail [19,23,24]. This response maintains the activity of S6K1 preserving a high level of phosphorylation at Thr389, a hallmark of active S6K1 [19]. Hence in DEDD$^{-/-}$ mice, the activity of S6K1 was reduced in various cell types, and as observed in S6K1$^{-/-}$ mice, the insulin mass within pancreatic islets is reduced, resulting in overt glucose intolerance [19].

Having discovered the functional association of DEDD with S6K1, we here address a possible interaction of DEDD with Akt, and investigate a novel involvement of DEDD in the regulation of the insulin signaling cascade.

Material and methods

Mice. DEDD$^{-/-}$ mice [21] had been backcrossed to C57BL/6 (B6) for 17 generations before used for experiments. Mice are maintained under a SPF condition.

Antibodies. Antibodies used are: anti-total Akt (clone 11E7), anti-Akt phosphorylated at Thr308 (clone 244F9) (all are from Cell Signaling Technology, Beverly, MA); anti-Hsp90 (clone SPA-830) and anti-Cdk1 (clone A17) (from Stressgen, Victoria, BC, Canada, and Zymed Laboratories Inc., South San Francisco, CA).

Glucose incorporation. This assay was performed as described previously [25] with some modifications. Pieces from epididymal white fat pads and the soleus muscles of the mice were used. To determine 2-DG uptake, the muscles and fat pads were transferred to buffer A containing 1 mM 2-DG (0.5 μCi/ml 2-deoxy-D-[1-^{14}C]glucose) and 1 mM L-glucose (5 μCi/ml L-[1-^{3}H]glucose) with or without 10 nM insulin and incubated at 30 °C for 10 min. After the reaction is terminated, the samples were neutralized with 5 N HCl and dissolved in ACSII (Amersham Biosciences). ^{14}C and ^{3}H specific activities were counted by a liquid scintillation counter (Packard Instrument Co.).

GLUT4 translocation. Primary MEF cells prepared from DEDD$^{+/+}$ or DEDD$^{-/-}$ embryos were differentiated to adipocytes according to established protocols [26]. GLUT4 translocation assay was performed as previously described [26,27], using a GFP-fused GLUT4 expression vector [27]. Confluent primary MEF cells prepared from DEDD$^{+/+}$ or DEDD$^{-/-}$ mice were induced to differentiate by incubating the cells with DMEM containing 10 μg/ml of insulin (Sigma), 1 μM of dexamethasone (Sigma), and 500 μM of isobutylmethylxanthine (Sigma). After 48 h, the cells were fed with DMEM containing 10 μg/ml of insulin every 2 days prior to use. On 8–10 days after induction of differentiation, cells were transfected with the construction cording GFP-GLUT4-myc [27]. Cells were serum-starved for 4 hours, and then incubated with or without 200nM of insulin for 30 min. GFP-GLUT4 trafficking was followed by a fluorescent microscope. A ratio for GFP-GLUT4 distribution within peri-membrane areas to peri-nuclear areas was measured using NIH-Image.

Na_3VO_4 treatment. DEDD$^{+/+}$ or DEDD$^{-/-}$ MEF cells were enriched in metaphase by a treatment with 500 nM nocodazole (Sigma) for 24 h. Cells were further incubated with 10 mM Na_3VO_4 for an additional 6 h, and lysed in SDS sample buffer. The cell extracts were subjected to Western blotting using anti-Akt or anti-Hsp90 antibodies.

Protein degradation and phosphorylation assay. Subconfluent DEDD$^{+/+}$ or DEDD$^{-/-}$ MEF cells were cultured accordingly and harvested at indicated time points after treatment with 100 μg/ml cyclohexamide with or without 10 μM MG-132 and 0.4 mM chloroquine, lysed with Briji 97 lysis buffer supplemented with 5 mM iodoacetamide, 5 μg/ml leupeptin, 0.2 mM AEBSF, 1 mM Na_3VO_4, and 10 mM NaF. Lysates were resolved onto SDS–PAGE, and immunoblotted anti-Akt antibody.

siRNA transfection. Double strands siRNA targeting DEDD or Cdk1 were purchased from Applied Biosystems or SIGMA, respectively. Wild-type MEF cells at 50% confluency were transfected with 10 μM siRNA using Lipofectamine 2000 (Invitrogen Inc.). Forty-eight hours after the transfection, the cells were harvested and analyzed by Western blotting or RT-PCR. Sequences of the oligonucleotides were as follows: DEDD siRNA#1: 5′-GCCCTGATC TTGTAGACAATT-3′, DEDD siRNA#2: 5′-AAATGGACGTGACTTCTTA TT-3′, Cdk1 siRNA#1: 5′-CTATGATCCTGCCAAACGATT-3′, Cdk1 siRNA#2: 5′-GTTGTTTACCGTTGGCTCTTT-3′, Cdk1 siRNA#3: 5′-CAATC AAACTGGCTGATTTTT-3′. For a control, an oligonucleotide targeting GFP sequence (Sigma) was used.

Primers for RT-PCR. Primers used are as follows: for, forward primer; rev, reverse primer. Hsp90α for: 5′-GCGGCAAAGACAAGAAA AAG-3′; Hsp90α rev: 5′-CAAGTGGTCCTCCCAGTCAT-3′; Hsp90β for: 5′-CTGGGTCAAGCAGAAAGGAG-3′; Hsp90β rev: 5′-TCTCTGTTG CTTCCCGACTT-3′; Akt1 for: 5′-CCACGCTACTTCCTCCTC-3′; Akt1 rev: 5′-TGCCCTTGCCAACAGTCTGAAGCA-3′; Akt2 for: 5′-GTCGCC AACAGTCTGAAGCA-3′; Akt2 rev: 5′-GAGAGAGGTGGAAAAACAG C-3′; G3PDH for: 5′-ACCACAGTCCATGCCATCAC-3′; G3PDH rev: 5′-TCCACCACCCTGTTGCTGTA-3′; β-actin for: 5′-GTGGCTACAGCTTC ACCACCACAG-3′; β-actin rev: 5′-GCATCCTGTCAGCAATGCCTGGG T-3′; DEDD for: 5′-GCGGGATCCGCGGGCCTAAAGAGGC-3′; DEDD rev: 5′-GCGTCTAGAGTCTACAAGATCAGGGC-3′.

Quantification of immuno-blots. Quantification of the immunoblots was performed using the NIH-Image. Relative phosphorylation levels to those in control (shown as 1.0 ± SEM) are presented. For all immuno-blotting experiments, at least three independent blotting were performed.

Statistical analysis. A two-tailed Mann–Whitney test was used to calculate *P*-values. (**): $P < 0.01$, (*): $P < 0.05$. Error bars: SEM.

Results

Lack of DEDD decreases the amount of Akt protein

Having observed reduced activity of S6K1 in the absence of DEDD [19], we wondered whether upstream of S6K1 in the insulin signalling pathway might also be influenced by the lack of DEDD, and thus assessed the situation of Akt protein in DEDD$^{-/-}$ mouse embryonic fibroblast (MEF) cells by Western blotting. To our surprise, the amount of Akt was also greatly decreased in DEDD$^{-/-}$ MEF cells compared with DEDD$^{+/+}$ MEF cells, when tested by using an antibody that detects all isotypes of Akt (Fig. 1A, total Akt). Signals for activated Akt phosphorylated at Thr308 residue were also reduced, along with the diminished amounts of total Akt protein (Fig. 1A, p-Akt). A reduction in the amount of Akt as well as in the Thr308 phosphorylation level, was also clear in DEDD$^{-/-}$ skeletal muscles and adipose tissues, where Akt plays an important role in the regulation of glucose homeostasis [12,13] (Fig. 1B). The effect of an acute loss of DEDD on Akt was also assessed by knocking down DEDD in cells. As presented in Fig. 1C, downregulation of DEDD expression by introducing a double-stranded siRNA for DEDD into wild-type MEF cells significantly reduced the amount of Akt. Consistent with these observations, the activating phosphorylation (at Ser2448) of mTOR, downstream of Akt, was decreased in DEDD$^{-/-}$ compared with DEDD$^{+/+}$ cells (Fig. 1D, left). In contrast, phosphorylation levels of 3-phosphoinositide-dependent protein kinase-1 (PDK1), which phosphorylates Akt, were comparable in the presence or absence of DEDD, suggesting that the less phosphorylation of Akt in the absence of DEDD is mainly caused by a reduction in the total amount of Akt protein (Fig. 1E). Together, the lack of DEDD decreases the amount of all types of Akt protein both in MEF cells and in tissues from DEDD$^{-/-}$ mice, which is accompanied with lower Akt activity. This

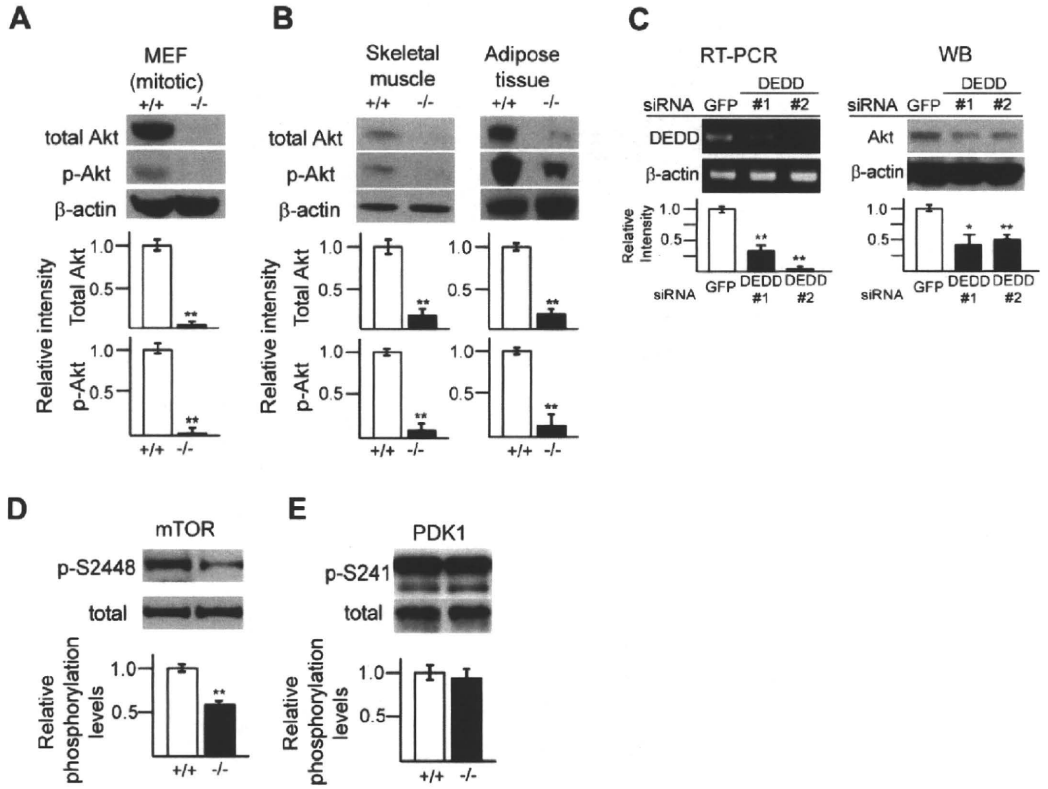

Fig. 1. Reduced Akt protein amounts in the absence of DEDD. (A) Total Akt or phosphorylated (activated) Akt analyzed in DEDD$^{+/+}$ and DEDD$^{-/-}$ MEF cells, and (B) in tissues from DEDD$^{+/+}$ and DEDD$^{-/-}$ mice. The representative immuno-blots and the averages of relative intensities (+/+ as 1.0) from all experiments are presented. Error bar: SEM. (C) Increase of Akt levels by diminishment of DEDD using siRNA in DEDD$^{-/-}$ MEF cells. DEDD mRNA and Akt protein levels relative to those in control (shown as 1.0) are also presented. (D) Activative phosphorylation of mTOR (at Ser2448 site) and (E) PDK1 (at Ser241 site) in DEDD$^{+/+}$ or DEDD$^{-/-}$ MEF cells was analyzed by Western blotting. For PDK1, two bands appear when this polyclonal antibody (Cell signalling; #3061) is used as described in its data sheet provided from the company. The upper band is the phosphorylated PDK1. Three independent experiments (for both D and E) were performed.

result also indicates that in the absence of DEDD, the reduction in Akt activity may partly be responsible for the decreased S6K1 activity, in addition to the increased phosphorylation levels at the inhibitory residues of S6K1 brought about by the hyper activity of Cdk1 [19].

DEDD forms a complex with Akt and Hsp90, and stabilizes these proteins

Although the amount of Akt protein is markedly reduced, mRNA for both Akt1 and Akt2 were expressed at similar levels in DEDD$^{-/-}$ and DEDD$^{+/+}$ tissues and cells (Fig. 2A). This result suggests that DEDD may be necessary for the maintenance of Akt protein. To test this possibility, we measured the half-life of Akt protein in DEDD$^{-/-}$ and DEDD$^{+/+}$ MEF cells. Importantly, the amount of Akt protein was decreased in 10 hours in DEDD$^{-/-}$ cells, but not in DEDD$^{+/+}$ cells (Fig. 2B). The presence of MG-132, a proteasome inhibitor, tempered the reduction observed in DEDD$^{-/-}$ cells (Fig. 2B). Thus, the lack of DEDD results in instability of Akt protein.

Several groups reported that heat-shock protein 90 (Hsp90), a chaperone required for the conformational maturation of certain signalling proteins, forms a complex with Akt and is involved in its stabilization [28,29]. Thus, we assessed the protein levels of Hsp90 in DEDD$^{+/+}$ and DEDD$^{-/-}$ MEF and tissues. As depicted in Fig. 2C, the amount of Hsp90 protein also decreased in skeletal muscle, adipose tissue, as well as in MEF cells from DEDD$^{-/-}$ mice compared with those from DEDD$^{+/+}$ mice, whereas the transcripts of *Hsp90* (both α and β) genes were at an equivalent level in both types of mice (Fig. 2D). Furthermore, as depicted in Fig. 2E, immunoprecipitation assays revealed that DEDD associates with Akt (both 1 and 2) and Hsp90. Together, DEDD appears to facilitate a stable complex with Akt and Hsp90, supporting the levels of these proteins.

Suppression of Cdk1 increases Akt protein levels in DEDD$^{-/-}$ cells

As we demonstrated in a previous report, DEDD modulates the activity of S6K1 partly via suppressing Cdk1 activity [19]. To assess whether the inhibitory effect of DEDD on Cdk1 is also involved in stabilizing Akt protein, we knocked down Cdk1 in DEDD$^{-/-}$ MEF cells by introducing double-stranded siRNA for Cdk1, and analyzed the Akt and Hsp90 protein levels. As demonstrated in Fig. 3A, the levels of both proteins increased in DEDD$^{-/-}$ cells when Cdk1 protein was diminished. In addition, treatment of DEDD$^{-/-}$ MEF cells with sodium orthovanadate (VO_4), which is commonly used to inactivate Cdk1 [24], significantly increased the levels of both Akt and Hsp90 (Fig. 3B). These data suggest that in DEDD$^{-/-}$ cells, the increase in Cdk1 activity appeared to be responsible to the instability of Akt protein.

Attenuated glucose incorporation in DEDD$^{-/-}$ skeletal muscles and adipose tissues

One of a variety of functions for Akt is the regulation of incorporation of glucose into cells in response to insulin [30–32]. It is well known that translocation of GLUT4 to the plasma membrane upon insulin stimulation is a key mechanism of glucose transport into cells [12,13], and that this translocation of GLUT4 is dependent on activation of Akt, in particular Akt2 [33–35]. Therefore, we assessed how the reduction of the amount of Akt caused by the ab-

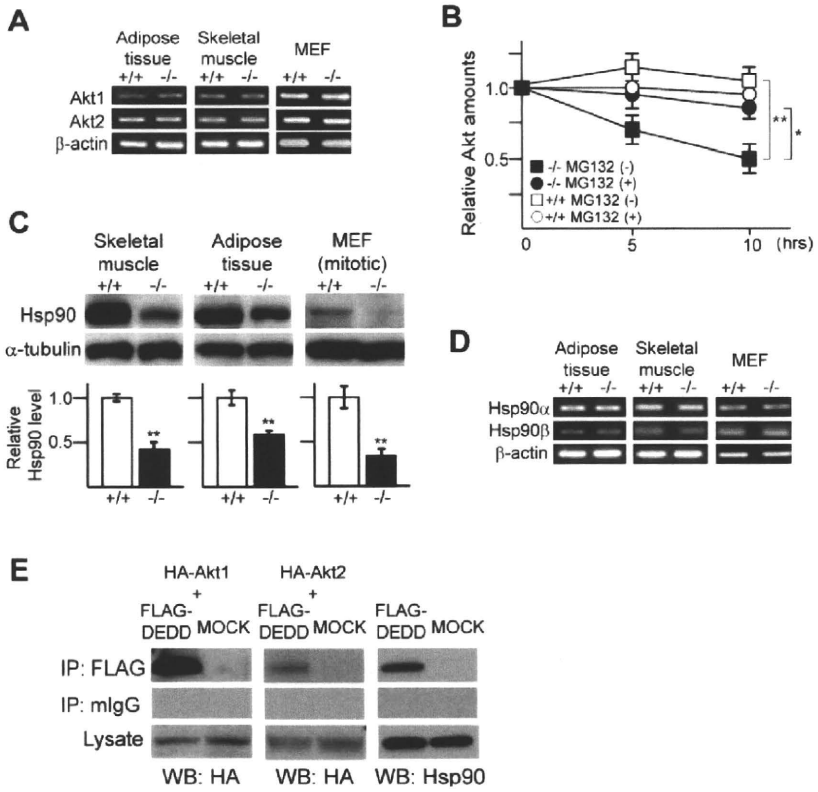

Fig. 2. DEDD forms a complex with Akt and Hsp90 and supports the stability of these proteins. (A) RT-PCR for Akt1, Akt2, and β-actin as a control (performed within the linear range). (B) Protein degradation assay for Akt. Representative data out of comparable results obtained by two independent experiments is presented. (C) Hsp90 protein levels in DEDD$^{+/+}$ or DEDD$^{-/-}$ skeletal muscle, adipose tissue or mitotic MEF cells. (D) RT-PCR assay for Hsp90 mRNA. (E) Association of DEDD with Akt1, Akt2, and Hsp90. DEDD was precipitated from 293T cells expressing HA-tagged AKt1 or Akt2 with or without FLAG-DEDD, and the precipitates were analyzed for HA-Akt1 or 2 using an anti-HA antibody (left and middle). Likewise, endogenous Hsp90 was co-precipitated with FLAG-DEDD from 293T cells expressing FLAG-DEDD (right). Results from the control IP using a mouse-IgG (mIgG) are also demonstrated.

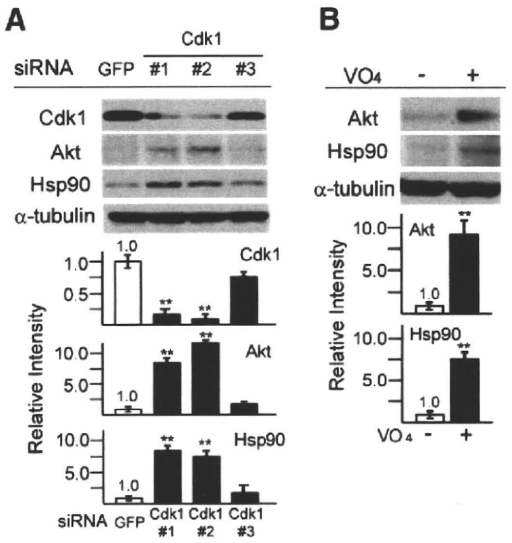

Fig. 3. Involvement of Cdk1 in stabilization of Akt by DEDD. (A) Akt and Hsp90 levels in mitotic DEDD$^{-/-}$ MEF cells after treatment with siRNA targeting Cdk1 (three distinct sequences), or (B) with Na_3VO_4 (VO_4) for 6 h. The levels of Akt and Hsp90 relative to those in control (shown as 1.0) are also presented.

sence of DEDD affects glucose uptake in mice. As shown in Fig. 4A, the uptake of glucose by skeletal muscle (soleus muscles) and adipose tissue in response to insulin was significantly damaged in DEDD$^{-/-}$ mice. We also tested GLUT4 translocation in response to insulin, using DEDD$^{-/-}$ and DEDD$^{+/+}$ adipocytes differentiated from MEF cells. The increase of GLUT4 on the cell membrane after an insulin challenge was significantly less in DEDD$^{-/-}$ compared to DEDD$^{+/+}$ cells (Fig. 4B). Hence, diminished levels of Akt correlated with inefficient induction of GLUT4 translocation, resulting in deficient glucose transport into cells in DEDD$^{-/-}$ skeletal muscle and adipose tissue.

Interestingly, however, Akt levels were almost comparable in the liver in DEDD$^{-/-}$ and DEDD$^{+/+}$ mice, in contrast to levels in skeletal muscle and adipose tissue (Fig. 4C). As the endogenous DEDD expression level was lower in the liver compared with that in the skeletal muscle (Fig. 4D), the loss of DEDD might not strongly influence Akt stability in the liver as it did in the skeletal muscle or adipose tissue.

Discussion

In addition to our previous report in which DEDD maintains the activity of S6K1 supporting the insulin mass within pancreatic islets, our current study has demonstrated that DEDD stabilizes Akt protein, leading to efficient glucose transport into skeletal muscles and adipose tissues. Thus, DEDD is involved in the insulin signalling pathway at diverse levels (summarized in Fig. 4E). As type 2 diabetes mellitus is a multifactorial disease [17], our findings suggest that DEDD-deficiency might play a certain role in the pathology of type 2 diabetes mellitus. Indeed, the defect in glucose transport observed in DEDD$^{-/-}$ mice is one of the essential pathogenic features in type 2 diabetes mellitus. Evidence has also

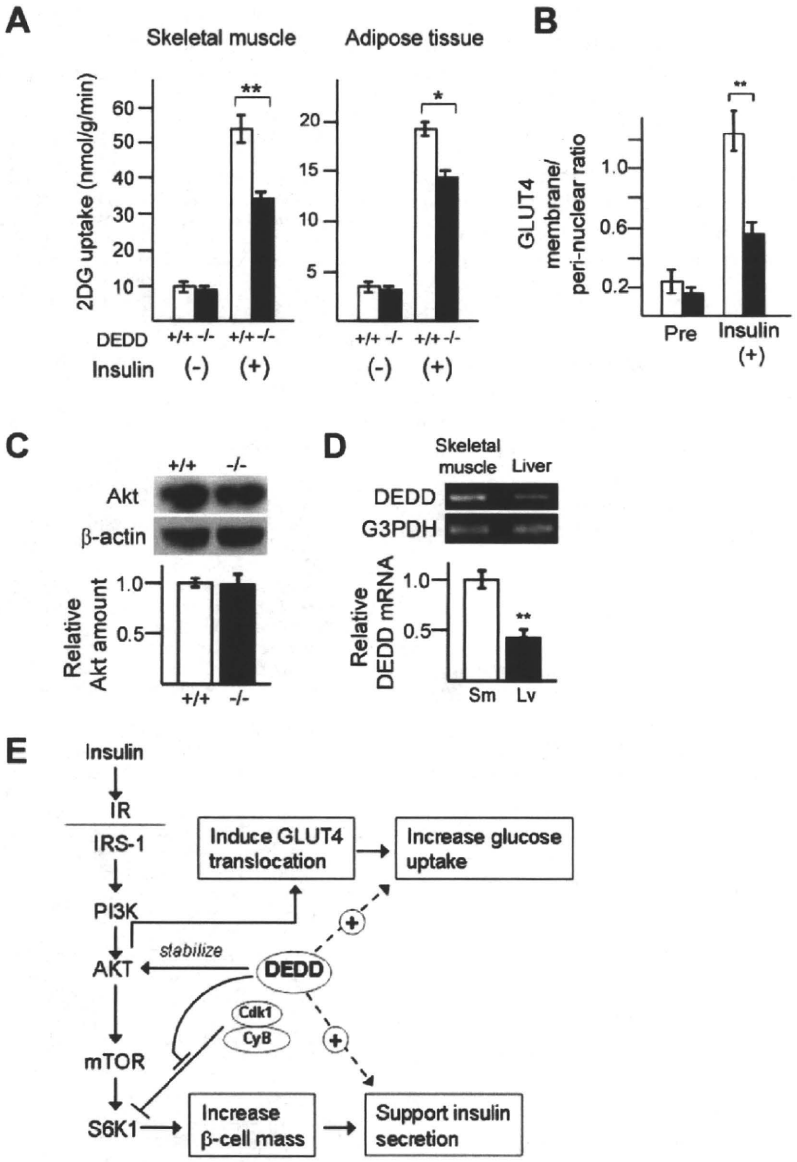

Fig. 4. Defects in glucose incorporation in DEDD$^{-/-}$ tissues. (A) Glucose incorporation by skeletal muscle (left) or adipose tissue (right) ($n = 5$ each). (B) Translocation of GLUT4 in DEDD$^{+/+}$ (white bars) or DEDD$^{-/-}$ (black bars) adipocytes. Data represent the relative amount of GFP-GLUT4 at the membrane locus to that at the peri-nuclear area. Data are the averages of results from 30 cells. (C) Akt protein levels in DEDD$^{-/-}$ and DEDD$^{+/+}$ liver. (D) DEDD mRNA level expressed in the liver (Lv) relative to that in the skeletal muscle (Sm) is presented (lower panel). (E) A scheme for the plausible involvement of DEDD in glucose homeostasis. IR, insulin receptor; CyB, cyclin B1. The + with a dashed line (that starts from DEDD) means positive effect.

shown that a decrease in insulin secretion and reduced β cell mass do contribute to development of the disease [16,18].

It is interesting that the decrease in Akt protein levels was variable in different DEDD$^{-/-}$ tissues important for glucose homeostasis; i.e. it was prominent in the skeletal muscles and adipose tissues, but was not very significant in the liver. This might cause a variable aberrancy in glucose transport in different organs in DEDD$^{-/-}$ mice. Additional experiments such as to test the insulin sensitivity in each tissue, will test this possibility. It may be noteworthy that such a variation in insulin sensitivity in different tissues is often seen in human patients [16–18]. It will also be important to address whether any dysfunction of DEDD is present, either in the whole body or in specific tissues, in a subset of type 2 diabetes patients.

The precise mechanism of how the association of DEDD with Akt and Hsp90 supports the stability of these proteins is still unclear. The DEDD's effect on Akt stability appears to be achieved through Cdk1. As we previously demonstrated, increased Cdk1 activity in the absence of DEDD accelerates the phosphorylation levels at the inhibitory residues of S6K1, resulting in a reduction of S6K1 activity [19]. A similar scenario might also be true for Akt (and/or Hsp90), although so far, inhibitory phosphorylation sites are not known either in Akt or Hsp90. Otherwise, Cdk1 might phosphorylate and activate some ubiquitin ligase(s) that degenerate Akt. As reviewed by Hunter [36], multiple crosstalks between phosphorylation and ubiquitination occur differentially during the protein degradation. Phosphorylation can regulate ubiquitination of a protein in different manners. Firstly, phosphorylation positively or negatively regulates the activity of the E3 ligase responsible for ubiquitine transfer. It is possible that Cdk1 may phosphorylate some E3 ligase(s) responsible for ubiquitination and degradation of Akt. Indeed, some E3 ligases involved in degradation of Akt, including recently identified TTC3 [37], require phosphorylation for their activation. Whilst, activity of CHIP, a major E3

ligase responsible for ubiquitination of Akt [38,39], might be modified directly or indirectly by Cdk1-depedent phosphorylative events, though the direct phosphorylation of CHIP has not been reported. On the other hand, it is also known that phosphorylation also promotes recognition of substrates by an E3 ligase [40]. However, phosphorylation events of Akt promoted by Cdk1 have not yet demonstrated. Alternatively, the possibility that formation of DEDD/Akt/Hsp90 might structurally stabilize these participant proteins is not mutually excluded. Thus, the molecular linkage among DEDD, Cdk1 and Akt-degradation still remains to be further addressed.

Conclusions

In summary, we newly demonstrated that DEDD plays an important role in maintenance of the Akt protein level, which in consequence supports the efficient incorporation of glucose into skeletal muscles and adipose tissues. Further investigations might find an unknown relevance of DEDD to the insulin signalling pathway, and thus, with a novel pathogenesis of type 2 diabetes mellitus.

Acknowledgments

We thank to Drs. T. Kubota, T. Kadowaki, T. Ide, K. Murakami, F. Suizu, M. Noguchi for technical assistance and useful discussion; Drs. S. Nishimura and M.P. Czech for the GFP-GLUT4 vector. This work was supported by Grants-in-Aid for Scientific Research (B) (Japan Society for the Promotion of Science), NIH (5RO1AI50948), Research Fund of Mitsukoshi Health and Welfare Foundation, Mitsubishi Pharma Research Foundation, (to T.M.), Kanae Foundation for the Promotion of Medical Science, Astellas Foundation for Research on Metabolic Disorders, and Ono Medical Research Foundation (to S.A.).

References

[1] E. Jacinto, M.N. Hall, Tor signalling in bugs, brain and brawn, Nat. Rev. Mol. Cell. Biol. 4 (2003) 117–126.
[2] S. Oldham, E. Hafen, Insulin/IGF and target of rapamycin signaling: a TOR de force in growth control, Trends Cell Biol. 13 (2003) 79–85.
[3] B. Valentinis, R. Baserga, IGF-I receptor signalling in transformation and differentiation, Mol. Pathol. 54 (2001) 133–137.
[4] P.K. Vogt, PI 3-kinase, mTOR, protein synthesis and cancer, Trends Mol. Med. 7 (2001) 482–484.
[5] D.C. Fingar, J. Blenis, Target of rapamycin (TOR): an integrator of nutrient and growth factor signals and coordinator of cell growth and cell cycle progression, Oncogene 23 (2004) 3151–3171.
[6] S. Huang, P.J. Houghton, Targeting mTOR signaling for cancer therapy, Curr. Opin. Pharmacol. 3 (2003) 371–377.
[7] F. Shamji, P. Nghiem, S.L. Schreiber, Integration of growth factor and nutrient signaling: implications for cancer biology, Mol. Cell 12 (2003) 271–280.
[8] Vivanco, C.L. Sawyers, The phosphatidylinositol 3-kinase AKT pathway in human cancer, Nat. Rev. Cancer 2 (2002) 489–501.
[9] M. Pende, S.C. Kozma, M. Jaquet, et al., Hypoinsulinaemia, glucose intolerance and diminished beta-cell size in S6K1-deficient mice, Nature 408 (2000) 994–997.
[10] S.G. Dann, A. Selvaraj, G. Thomas, mTOR complex1–S6K1 signaling: at the crossroads of obesity, diabetes and cancer, Trends Mol. Med. 13 (2007) 252–259.
[11] S.H. Um, D. D'Alessio, G. Thomas, Nutrient overload, insulin resistance, and ribosomal protein S6 kinase 1, S6K1, Cell Metab. 3 (2006) 393–402.
[12] M.M. Hill, S.F. Clark, D.F. Tucker, et al., A role for protein kinase Bbeta/Akt2 in insulin-stimulated GLUT4 translocation in adipocytes, Mol. Cell. Biol. 19 (1999) 7771–7781.
[13] S. Huang, M.P. Czech, The GLUT4 glucose transporter, Cell Metab. 5 (2007) 237–252.
[14] S.A. Summers, L.A. Garza, H. Zhou, M.J. Birnbaum, Regulation of insulin-stimulated glucose transporter GLUT4 translocation and Akt kinase activity by ceramide, Mol. Cell. Biol. 18 (1998) 5457–5464.
[15] E.L. Whiteman, H. Cho, M.J. Birnbaum, Role of Akt/protein kinase B in metabolism, Trends Endocrinol. Metab. 13 (2002) 444–451.
[16] G.I. Bell, K.S. Polonsky, Diabetes mellitus and genetically programmed defects in beta-cell function, Nature 414 (2001) 788–791.
[17] R.A. DeFronzo, Pathogenesis of type 2 diabetes: metabolic and molecular implications for identifying diabetes genes, Diabetes Rev. 5 (1997) 177.
[18] B.B. Kahn, L. Rossetti, Type 2 diabetes—who is conducting the orchestra?, Nat Genet. 20 (1998) 223–225.
[19] N. Kurabe, S. Arai, A. Nishijima, et al., The death effector domain-containing DEDD supports S6K1 activity via preventing Cdk1-dependent inhibitory phosphorylation, J. Biol. Chem. 284 (2009) 5050–5055.
[20] H. Stegh, O. Schickling, A. Ehret, et al., DEDD, a novel death effector domain-containing protein, targeted to the nucleolus, EMBO J. 17 (1998) 5974–5986.
[21] S. Arai, K. Miyake, R. Voit, et al., The death-effector domain containing protein DEDD is a novel mitotic inhibitor requisite for cell growth, Proc. Natl. Acad. Sci. USA 104 (2007) 2289–2294.
[22] T. Miyazaki, S. Arai, Two distinct controls of mitotic Cdk1/cyclin B1 requisite for cell growth prior to cell division, Cell Cycle 6 (2007) 1419–1425.
[23] P.J. Papst, .H. Sugiyama, M. Nagasawa, et al., Cdc2-cyclin B phosphorylates p70 S6 kinase on Ser411 at mitosis, J. Biol. Chem. 273 (1998) 15077–15084.
[24] O.J. Shah, S. Ghosh, T. Hunter, J. Biol. Chem. 278 (2003) 16433–16442.
[25] N. Kamei, K. Tobe, R. Suzuki, et al., Overexpression of monocyte chemoattractant protein-1 in adipose tissues causes macrophage recruitment and insulin resistance, J. Biol. Chem. 281 (2006) 26602–26614.
[26] S. Bogan, A.E. McKee, H.F. Lodish, Insulin-responsive compartments containing GLUT4 in 3T3-L1 and CHO cells: regulation by amino acid concentrations, Mol. Cell. Biol. 21 (2001) 4785–4806.
[27] Z.Y. Jiang, A. Chawla, A. Bose, et al., A phosphatidylinositol 3-kinase-independent insulin signaling pathway to N-WASP/Arp2/3/F-actin required for GLUT4 glucose transporter recycling, J. Biol. Chem. 277 (2002) 509–515.
[28] D. Basso, D.B. Solit, G. Chiosis, et al., Akt forms an intracellular complex with heat shock protein 90 (Hsp90) and Cdc37 and is destabilized by inhibitors of Hsp90 function, J. Biol. Chem. 277 (2002) 39858–39866.
[29] D.B. Solit, A.D. Basso, A.B. Olshen, et al., Inhibition of heat shock protein 90 function down-regulates Akt kinase and sensitizes tumors to Taxol, Cancer Res. 63 (2003) 2139–2144.
[30] D.P. Brazil, Z.Z. Yang, B.A. Hemmings, Advances in protein kinase B signalling: AKTion on multiple fronts, Trends Biochem. Sci. 29 (2004) 233–242.
[31] B.D. Manning, L.C. Cantley, AKT/PKB signaling: navigating downstream, Cell 129 (2007) 1261–1274.
[32] K. Du, P.N. Tsichlis, Regulation of the Akt kinase by interacting proteins, Oncogene 24 (2005) 7401–7409.
[33] H. Cho, J. Mu, J.K. Kim, J.L. Thorvaldsen, et al., Insulin resistance and a diabetes mellitus-like syndrome in mice lacking the protein kinase Akt2 (PKB beta), Science 292 (2001) 1728–1731.
[34] R.S. Garofalo, S.J. Orena, K. Rafidi, et al., Severe diabetes, age-dependent loss of adipose tissue, and mild growth deficiency in mice lacking Akt2/PKB beta, J. Clin. Invest. 112 (2003) 197–208.
[35] Y. Ng, G. Ramm, J.A. Lopez, D.E. James, Rapid activation of Akt2 is sufficient to stimulate GLUT4 translocation in 3T3-L1 adipocytes, Cell Metab. 7 (2008) 348–356.
[36] T. Hunter, The age of crosstalk: phosphorylation, ubiquitination, and beyond, Mol. Cell 28 (2007) 730–738.
[37] F. Suizu, Y. Hiramuki, F. Okumura, et al., The E3 ligase TTC3 facilitates ubiquitination and degradation of phosphorylated Akt, Dev. Cell 17 (2009) 800–810.
[38] C.A. Dickey, J. Koren, Y. Zhang, et al., Akt and CHIP coregulate tau degradation through coordinated interactions, Proc. Natl. Acad. Sci. USA 105 (2008) 3622–3627.
[39] V. Facchinetti, W. Ouyang, H. Wei, et al., The mammalian target of rapamycin complex 2 controls folding and stability of Akt and protein kinase C, EMBO J. 27 (2008) 1932–1943.
[40] T. Xiang, A. Ohashi, Y. Huang, et al., Negative Regulation of AKT Activation by BRCA, Cancer Res. 168 (2008) 10040–10044.

Intravital Imaging of IL-1β Production in Skin

Hironori Matsushima[1,2], Yasushi Ogawa[2], Toru Miyazaki[3], Hiroaki Tanaka[2], Akiko Nishibu[2] and Akira Takashima[1,2]

IL-1 is a prototypic inflammatory cytokine that has pathogenic roles in various skin disorders. Although Langerhans cells (LCs) have been reported to express IL-1β mRNA upon application of contact sensitizers, it remains unclear whether other cell types produce IL-1β in skin. Thus, we sought to directly identify IL-1β-producing cells in living animals by construction of transgenic mice expressing DsRed fluorescence protein gene under the control of IL-1β promoter. Little DsRed fluorescence signal was detected in skin under steady-state conditions. Striking increases in DsRed signal were observed after topical application of a contact sensitizer, oxazolone, which also induced markedly elevated IL-1β mRNA and protein expression. DsRed signal was expressed primarily by $CD45^+/CD11b^+$ myeloid leukocytes in both epidermal and dermal compartments and was detected only in small fractions of epidermal LCs. Interestingly, $DsRed^+$ cells emerged preferentially as clusters around hair follicles. Intravital confocal imaging experiments revealed highly motile potentials of $DsRed^+$ cells—they constantly crawled around hair follicles via amoeba-like movements with a mean velocity of $1.0 \pm 0.4\,\mu m\,min^{-1}$ (epidermis) or $2.7 \pm 1.4\,\mu m\,min^{-1}$ (dermis). The newly developed *in vivo* imaging system represents a useful tool for studying spatial regulation of IL-1β production in skin.

Journal of Investigative Dermatology (2010) **130,** 1571–1580; doi:10.1038/jid.2010.11; published online 11 February 2010

INTRODUCTION

Cytokines of the IL-1 family function as potent mediators and regulators of host inflammatory responses to infection and tissue injury. Of the 11 members of this family, IL-1β is the best-studied cytokine, with diverse phenotypes reported for IL-1β-deficient mice (Dinarello, 2009). On exposure to pathological stimuli, IL-1β is produced by activated leukocytes such as neutrophils, monocytes, macrophages, and dendritic cells (DCs) (O'Neill, 2008), leading to induction and enhancement of inflammatory responses. Bioactive IL-1β (18 kDa) is generated by caspase-1-dependent cleavage of an inactive precursor (31 kDa), pro-IL-1β (Cerretti *et al.*, 1992; Thornberry *et al.*, 1992). Recent studies have revealed that the inflammasome, the intracellular caspase-1-activating complex, serves as a key intracellular compartment for processing and secretion of bioactive IL-1β (Dinarello, 2009; Martinon *et al.*, 2009). Under inflammatory conditions, activation of the P2X7 receptor with extracellular ATP triggers the assembly of inflammasome components, resulting in the formation of active caspase-1 from procaspase-1. It should be stated, however, that pro-IL-1β may be processed in a caspase-1-independent manner by several proteases, such as neutrophil proteinase-3, elastase, matrix metalloprotease 9, and granzyme A, illustrating highly complex regulatory mechanisms (Fantuzzi *et al.*, 1997; Coeshott *et al.*, 1999; Sugawara *et al.*, 2001).

As an outermost tissue, the skin is constantly exposed to a variety of environmental insults, such as harmful chemicals, physical stimuli, and infectious microbes. It is well known that IL-1 functions as a key regulator of local host responses to such pathological stimuli. As early as in the early 1980s, an IL-1-like activity, termed the "epidermal cell-derived thymocyte-activating factor," was found to be produced in the skin (Luger *et al.*, 1982; Kupper *et al.*, 1986; Kupper, 1990). Primary cultures and cell lines derived from keratinocytes and Langerhans cells (LCs) in the epidermis, as well as from fibroblasts, endothelial cells, and DCs in the dermis, have been reported to produce IL-1α and/or IL-1β upon *in vitro* exposure to various stimuli (Enk and Katz, 1992; Takashima and Bergstresser, 1996). With regard to biological activities of IL-1 in skin, IL-1β-deficient mice were reported to manifest impaired contact hypersensitivity responses to trinitrochlorobenzene, which was applied topically for sensitization and injected into the footpad for elicitation (Shornick *et al.*, 1996; Nakae *et al.*, 2001; Nambu *et al.*, 2006). In a standard contact hypersensitivity model (in which trinitrochlorobenzene was applied topically for both sensitization and elicitation), however, reduced ear swelling responses were observed in IL-1α-deficient mice, but not in IL-1β-deficient mice (Shornick *et al.*, 1996; Nakae *et al.*, 2001; Nambu *et al.*, 2006). Conversely, the same group subsequently reported

[1]*Department of Medical Microbiology and Immunology, University of Toledo College of Medicine, Toledo, Ohio, USA;* [2]*Department of Dermatology, University of Texas Southwestern Medical Center, Dallas, Texas, USA and* [3]*Division of Molecular Biomedicine for Pathogenesis, Center for Disease Biology and Integrative Medicine, University of Tokyo, Tokyo, Japan*

Correspondence: Akira Takashima, Department of Medical Microbiology and Immunology, University of Toledo College of Medicine, 3000 Arlington Avenue, Toledo, Ohio 43614-5806, USA.
E-mail: akira.takashima@utoledo.edu

Abbreviations: BM, bone marrow; DC, dendritic cell; DX, dextran; LC, Langerhans cell; LPS, lipopolysaccharides; OX, oxazolone; WT, wild type

Received 18 September 2009; revised 2 December 2009; accepted 27 December 2009; published online 11 February 2010

significantly impaired delayed-type hypersensitivity responses to foreign protein antigens in IL-1β-deficient mice (Shornick *et al.*, 1996; Nakae *et al.*, 2001; Nambu *et al.*, 2006). Interestingly, severely attenuated contact hypersensitivity responses were also observed in caspase-1-deficient mice (Antonopoulos *et al.*, 2001; Watanabe *et al.*, 2007) and in wild-type (WT) mice after administration of neutralizing antibodies against IL-1β, but not against IL-1α (Enk *et al.*, 1993). Although relative contributions between IL-1α and IL-1β remain somewhat controversial, it is reasonable to state that IL-1 being produced in the skin serves as an indispensable proinflammatory mediator. Nevertheless, little information has been available with regard to spatiotemporal regulation of IL-1 production in living animals.

We recently found rapid and profound IL-1β promoter activation in DCs upon *in vitro* exposure to a variety of chemical and biological agents. In those studies, we used a 4.1 kb 5′-flanking fragment isolated from the murine IL-1β gene to drive the expression of the yellow fluorescence protein gene in a stably transduced DC clone. The resulting DC biosensor clone has enabled us to perform unbiased screening of a wide variety of natural and synthetic compounds for their potential to trigger IL-1β production (Mizumoto *et al.*, 2005). In this study, we sought to construct an *in vivo* reporter system by using the same IL-1β promoter to drive the expression of a fluorescence marker gene. The resulting transgenic mice, in combination with advanced intravital optical imaging technologies, have indeed allowed us to directly visualize IL-1β promoter activation in living animals. In this study, we report spatial regulation of IL-1β promoter activation, as well as the cellular identities and motile activities of IL-1β-producing cells in inflamed skin in an animal model.

RESULTS AND DISCUSSION

Detection of IL-1β promoter activation in hapten-painted skin

We generated a transgenic mouse line expressing the red fluorescent protein DsRed gene under the control of the 4.1 kb mouse IL-1β promoter. The pIL1-DsRed transgenic mice showed no apparent developmental abnormality. Topical application of a skin sensitizer, oxazolone (OX), a standard protocol widely used to trigger IL-1-dependent activation of epidermal-resident LCs (Cumberbatch *et al.*, 1997), triggered time-dependent IL-1β mRNA expression in the pIL1-DsRed transgenic mice (Figure 1a). The magnitude of IL-1β mRNA induction in these mice was comparable to that observed in WT mice (Figure 1b). Tissue extracts prepared from OX-painted ear skin showed large amounts of IL-1β proteins as measured by ELISA (Figure 1c). Time-course experiments showed rapid (6 hours) and robust IL-1β protein production in OX-painted skin with peak responses observed at 24 hours. Once again, pIL1-DsRed transgenic mice were indistinguishable from WT mice in the magnitude or kinetics of OX-induced IL-1β protein expression. No IL-1β mRNA or protein induction was detected after topical application of vehicle alone.

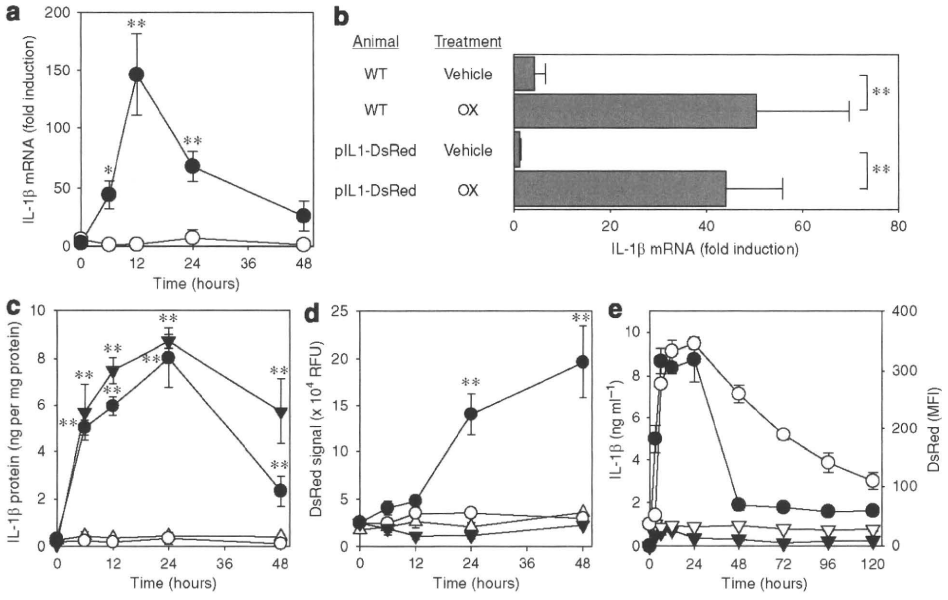

Figure 1. Correlation between DsRed fluorescence signals and IL-1β production. (**a**) pIL1-DsRed transgenic mice were treated by topical application of OX (closed symbols) or vehicle alone (open symbols). At the indicated time points, the ear skin samples were examined for IL-1β mRNA expression by real-time PCR. (**b**) Ear skin samples were isolated from WT mice or pIL1-DsRed transgenic mice 6 hours after topical application of OX or vehicle alone. The samples were then examined for IL-1β mRNA expression by real-time PCR. (**c**) WT mice (triangles) or pIL1-DsRed transgenic mice (circles) received topical application of OX (closed symbols) or vehicle alone (open symbols). At the indicated time points, the ear skin samples were examined for IL-1β protein levels by ELISA. (**d**) The same ear extract samples analyzed in panel **b** were tested for DsRed fluorescence signals by spectrophotometric analyses. (**e**) BM-DCs propagated from pIL1-DsRed transgenic mice were pulsed with LPS (circles) or vehicle alone (triangles) for 1 hour. After extensive washing, the cells were cultured for the indicated periods in the absence of LPS to measure IL-1β release into the culture supernatants by ELISA (closed symbols) and DsRed expression (mean fluorescence intensity, open symbols) by flow cytometry. Data shown are the means ± SD from three mice per group (**$P<0.01$).

To determine whether OX treatment also triggered IL-1β promoter-driven DsRed expression, we measured DsRed fluorescence signals in the same ear skin extracts by a spectrophotometer (Figure 1d). Minimal fluorescence signals were detected in ear skin samples treated with vehicle alone. OX treatment markedly increased DsRed signals in 12–24 hours, with peak responses observed at 48 hours. No significant increase in DsRed signals was detected in WT mice even after OX application, indicating specificity. Although the time kinetics for DsRed induction in skin showed a lag time of 6–12 hours behind IL-1β protein expression, which presumably represents the interval required for polymerization of newly synthesized DsRed proteins, our findings validated the subsequent use of the newly generated transgenic mice for studying IL-1β promoter activation in living animals.

The discordance of time kinetics observed between IL-1β protein production and DsRed expression might prevent us from studying the resolution phase of inflammatory responses. To test this, we compared time kinetics of IL-1β protein production versus DsRed signals in bone marrow–derived DCs (BM-DCs) propagated from pIL1-DsRed transgenic mice (Figure 1e). Short-term pulsing with LPS induced rapid IL-1β protein production within 3 hours; IL-1β levels reached a peak at 6–24 hours and then declined sharply at 48 hours, with a relatively short half-life of 24 hours. By contrast, DsRed signals became detectable only at 6 hours, reached a plateau at 12–24 hours, and then declined more slowly, with an estimated half-life of 24–48 hours. These observations imply a major limitation of our experimental system; i.e., one can assess IL-1β protein production by measuring DsRed fluorescence signals only in the induction phase of inflammation.

Surface phenotypes of DsRed$^+$ cells emerging in inflammatory skin lesions

Enk and Katz (1992) reported almost two decades ago that topical application of contact sensitizers triggered rapid and abundant IL-1β mRNA expression in the epidermal compartment and that IL-1β mRNA was expressed predominantly by an MHC class II–positive epidermal cell fraction, i.e., LCs. The latter observation was made by measuring IL-1β mRNA expression by semiquantitative RT-PCR in epidermal cell suspensions after complement-mediated deletion of MHC class II–positive cells. To directly examine cell-surface phenotypes of cells expressing DsRed fluorescence signals, we harvested ear skin samples at different time points after OX painting, separated the epidermis from underlying dermis by enzymatic treatment, and then prepared single-cell suspensions from the two compartments independently. Flow cytometric analyses of the resulting epidermal cell suspensions revealed a time-dependent increase in the number of DsRed$^+$ cells, with a sharp peak observed at 48 hours after OX treatment (Figure 2a). Most (>85%) of the DsRed$^+$ cells isolated from the epidermis were found to express a common leukocyte marker, CD45, although a small fraction of CD45$^-$ epidermal cells (i.e., keratinocytes) showed DsRed signals at modest levels (Figure 2b). The CD45$^+$ cells recovered before OX treatment, which represent two epidermal resident leukocyte populations (LCs and epidermal γδ T cells), expressed no detectable DsRed signals constitutively. The number of CD45$^+$ cells markedly increased after OX treatment, perhaps reflecting immigration of inflammatory leukocytes into the epidermal compartment. Importantly, DsRed signals were clearly detected in large fractions (53–61%) of the CD45$^+$ cells recovered after OX painting. Virtually all DsRed$^+$/CD45$^+$ cells expressed CD11b, which is displayed by many leukocyte subsets of the myeloid lineage (Figure 2c). More than 75% of the DsRed$^+$/CD45$^+$ cells also displayed high levels of Gr-1, a conventional marker of neutrophils. Although the overall phenotype of the CD45$^+$/CD11b$^+$/Gr-1^{high} cells instantaneously suggested their identity as granulocytes, some of them may represent "myeloid suppressors" (which inhibit DC-induced T-cell activation) (Gabrilovich and Nagaraj, 2009) and/or "inflammatory monocytes" (which give rise to DCs) (Auffray *et al.*, 2009). The remaining DsRed$^+$/CD45$^+$/Gr-1$^{-/low}$ cells probably included monocytes/macrophages and certain DC subsets. In fact, F4/80 and MHC class II molecules were detected on relatively small fractions of the CD45$^+$/DsRed$^+$ cells (Figure 2c). These results implied that DsRed signals were produced by selected subsets of myeloid inflammatory leukocytes infiltrating the epidermis after OX painting.

Dermal cell suspensions prepared in parallel also showed time-dependent increases in the number of DsRed$^+$ cells with a sharp peak at 48 hours (Figure 3a). Virtually all of the DsRed$^+$ cells recovered from the dermal compartment also expressed CD45 (Figure 3b). Moreover, the CD45$^+$/DsRed$^+$ cells uniformly displayed CD11b, indicating their myeloid origin (Figure 3c). Interestingly, only small fractions (18–20%) of the DsRed$^+$/CD45$^+$ cells expressed Gr-1 at high levels, in contrast to our observations of the epidermal cell suspensions. Instead, Gr-1 was detected at low levels in a majority (65–75%) of the DsRed$^+$/CD45$^+$ cells. Similarly, F4/80 and MHC class II were detected in 36–46% and 10–12% of the DsRed$^+$/CD45$^+$ cells, respectively. Thus, it seems that DsRed signals were expressed by relatively heterogeneous leukocyte subsets of myeloid origin (i.e., granulocytes, monocytes/macrophages, and DCs) in the dermal compartment after OX painting.

Detection of DsRed$^+$ cells in fixed skin samples

In the next set of experiments, we sought to directly visualize the cells expressing DsRed fluorescence signals in the tissue. For this purpose, we harvested ear skin at different time points after OX application, fixed the samples with paraformaldehyde, and then examined the whole-ear specimens under a macro-zoom fluorescence microscope. Consistent with our findings from spectrophotometric and flow cytometric analyses, very few DsRed$^+$ cells were found in skin samples harvested before OX painting from pIL1-DsRed transgenic mice. DsRed$^+$ cells became clearly detectable 12 hours after OX treatment (Figure 4a). Interestingly, most DsRed$^+$ cells emerged as clusters around hair follicles. The number of DsRed$^+$ cells increased thereafter, reaching a peak at 48 hours. Consistent with our observations in spectrophotometry and flow cytometry analyses, the DsRed signals

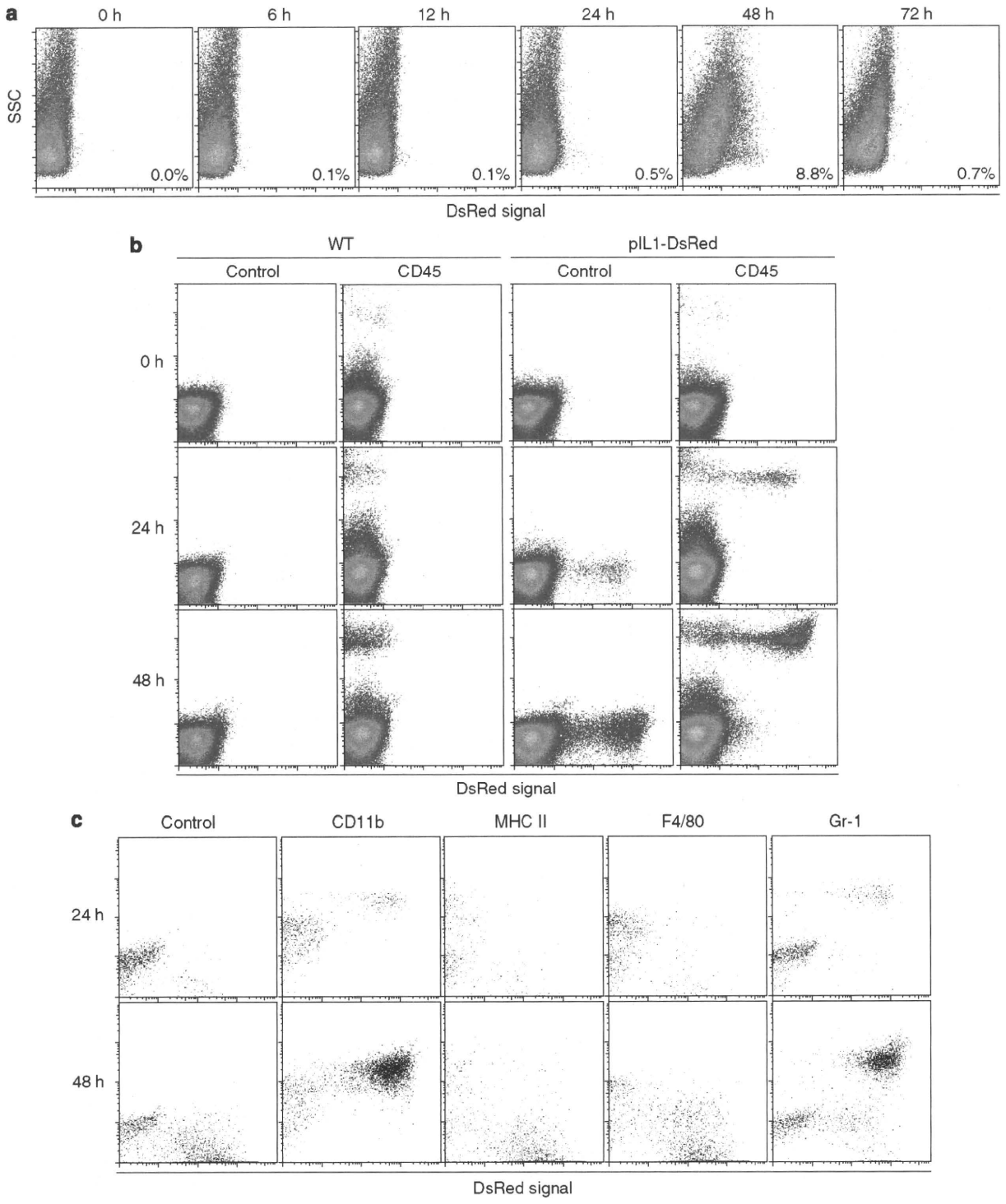

Figure 2. Surface phenotype of DsRed$^+$ cells emerging in the epidermal compartment. (**a**) Epidermal cell suspensions were prepared from the ear skin of pIL1-DsRed transgenic mice at the indicated time points after topical application of OX and examined for DsRed expression. (**b**) Epidermal cell suspensions from WT mice or pIL1-DsRed transgenic mice were also stained with anti-CD45 mAb or isotype-matched control IgG and then examined for expression of CD45 (*y* axis) and DsRed (*x* axis). (**c**) The CD45$^+$ populations in the above experiments were examined for the expression of the indicated surface markers (*y* axis) and DsRed (*x* axis).

declined sharply at 72 hours. No DsRed$^+$ cells were observed in WT mice even after OX painting, again indicating specificity (Figure 4b). Clusters of DsRed$^+$ cells were also observed after topical application of a second contact sensitizer, 2,4-dinitrofluorobenzene (Figure 4c). Moreover, inflammatory skin lesions induced by application

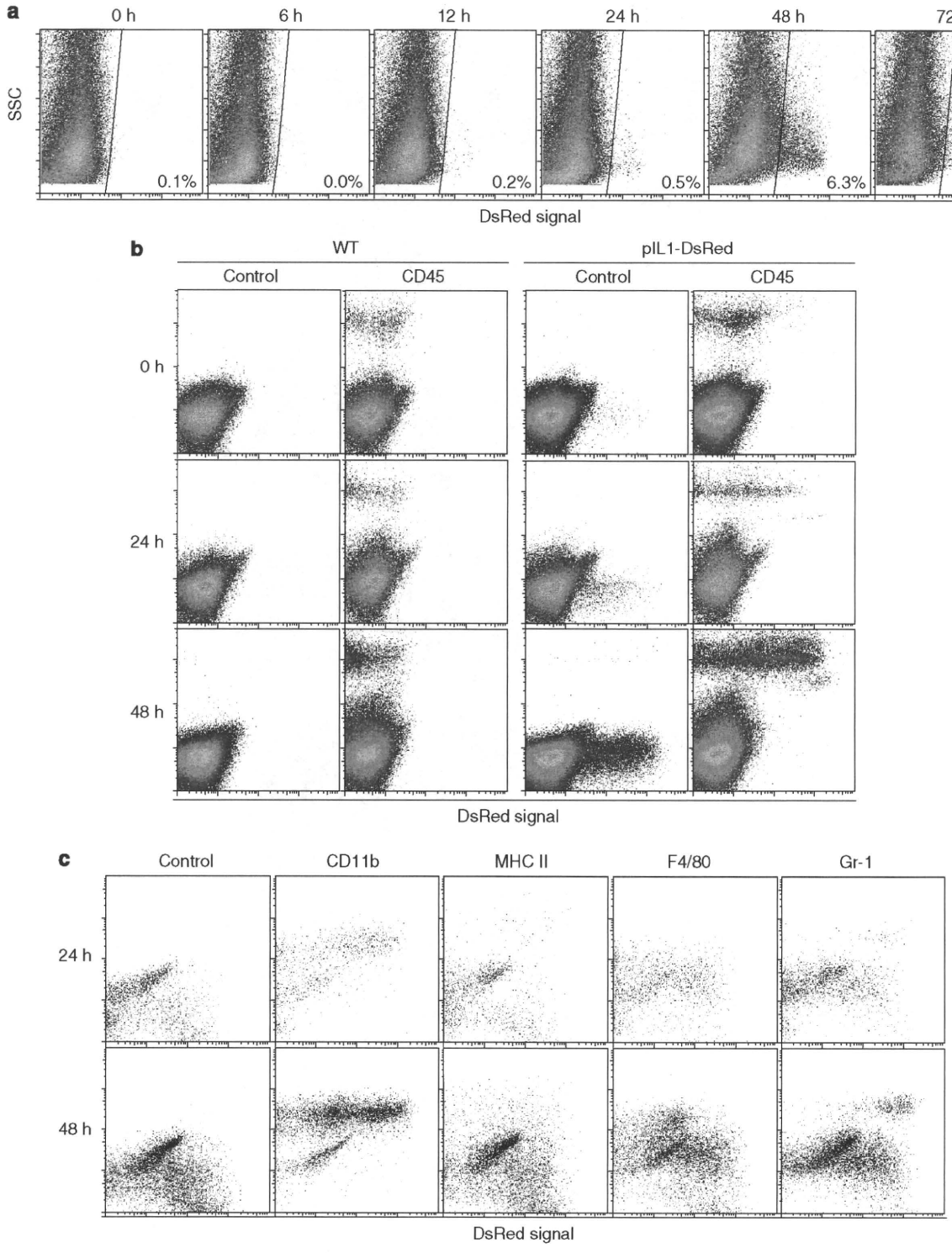

Figure 3. Surface phenotype of DsRed$^+$ cells emerging in the dermal compartment. (**a**) Dermal cell suspensions were prepared from the ear skin of pIL1-DsRed transgenic mice at the indicated time points after topical application of OX and examined for DsRed expression. (**b**) Dermal cell suspensions from WT mice or pIL1-DsRed transgenic mice were also stained with anti-CD45 mAb or isotype-matched control IgG and then examined for expression of CD45 (*y* axis) and DsRed (*x* axis). (**c**) The CD45$^+$ populations in the above experiments were examined for the expression of the indicated surface markers (*y*-axis) and for DsRed (*x* axis).

of a skin irritant, lactic acid, or by repeated tape stripping were also characterized by the emergence of large numbers of DsRed$^+$ cells.

To record images of DsRed$^+$ cells with higher resolution and to determine their *z*-axis locations, we next examined paraformaldehyde-fixed ear specimens under a confocal

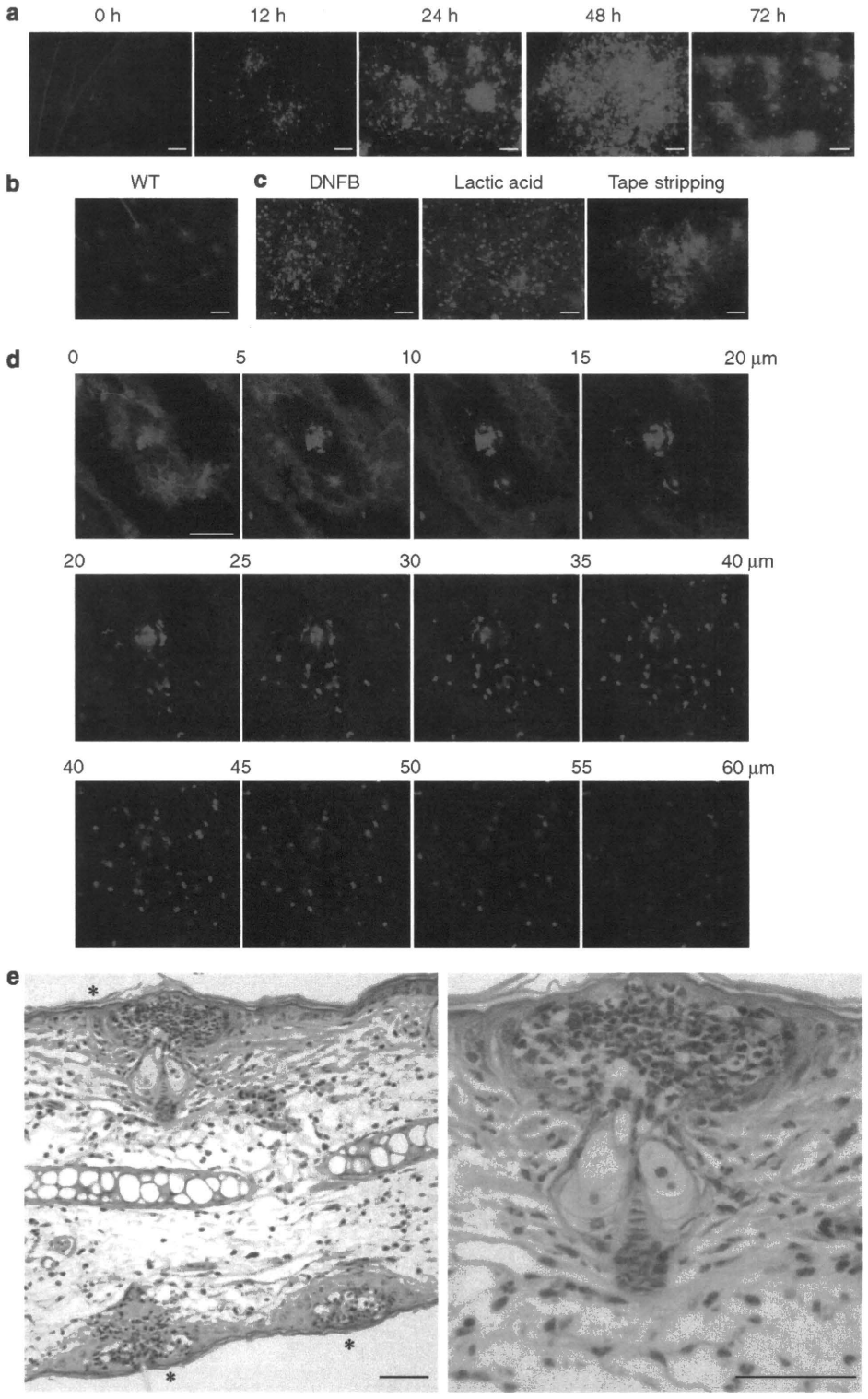

Figure 4. Emergence and distribution of DsRed$^+$ cells in skin under inflammatory conditions. (**a**) At the indicated time points after OX treatment of pIL1-DsRed transgenic mice, ear skin samples were harvested. Data shown are images acquired with a macro-zoom fluorescence microscope. (**b**) WT mice were treated with OX, and the ear skin samples harvested at 24 hours were examined under a macro-zoom fluorescence microscope. (**c**) pIL1-DsRed transgenic mice were treated with topical application of 2,4-dinitrofluorobenzene or lactic acid, or with repeated tape stripping. The ear skin samples harvested at 24 hours were examined under a macro-zoom fluorescence microscope. Bar (**a–c**) = 1,000 μm. (**d**) At 24 hours after OX treatment of pIL1-DsRed transgenic mice, the ear skin samples were harvested, fixed with 2% paraformaldehyde, and then examined under a confocal microscope. Data shown are compiled *x–y* plane images of DsRed$^+$ cells in the indicated 5 μm *z*-axis depth range from the skin surface. (**e**) Hematoxylin and eosin histology of ear skin samples harvested 24 hours after OX painting. Asterisks indicate hair follicles. Bar = 100 μm.

microscope (Figure 4d). Sequential *x–y* plane images scanned at different *z*-axis levels revealed that some keratinocytes showed DsRed fluorescence signals at marginal levels, producing cobblestone-like patterns in the epidermal compartment (up to ~20 μm in depth from the skin surface). Within the epidermis, DsRed$^+$ signals appeared as small aggregates associated with hair shafts, which were readily identifiable with autofluorescence signals. Interestingly, a small number of dendritic-shaped epidermal cells characterized by extension of several elongated processes exhibited strong DsRed signals. In the dermal compartment, most DsRed$^+$ cells were preferentially found around hair follicles at the *z*-axis depth range from ~20 to ~50 μm. Hematoxylin and eosin staining of vertical sections revealed multiple foci of dense infiltration by mononuclear and polymorphonuclear leukocytes around hair follicles in OX-treated ear skin (Figure 4e).

Real-time visualization of motile behaviors of DsRed$^+$ cells in living animals

To visualize IL-1β-producing cells in living tissue, we anesthetized pIL1-DsRed transgenic mice and recorded static 3D images of DsRed$^+$ cells in the OX-painted ear skin under a confocal microscope. Once again, compiled *x–y* plane images showed clusters of DsRed$^+$ cells preferentially around hair follicles (Figure 5a), and *z*-axis scanning and 360° rotation of the images further revealed that most of the DsRed$^+$ cells were located in the dermal compartment (see Supplementary Movies S1–S3 online). Once again, relatively small numbers of DsRed$^+$ cells showing a characteristic morphology of LCs were observed in the epidermal compartment (Supplementary Movie S2). Thus, we concluded that inflammatory leukocytes account for a majority of DsRed$^+$ cells emerging in the inflamed skin of living animals.

A key question was whether the observed clusters of DsRed$^+$ cells around hair follicles might be caused simply by particularly "leaky" blood vessels in those anatomical sites. To test this, we intravenously injected FITC-dextran (DX) into pIL1-DsRed transgenic mice 24 hours after OX painting on the ear. As shown in Figure 5b, significantly dilated blood vessels were readily observed in OX-treated skin, whereas leakage of FITC-DX was noticed only occasionally. Another concern was whether the experimental procedures used for confocal imaging (i.e., laser excitation, tissue handling, and

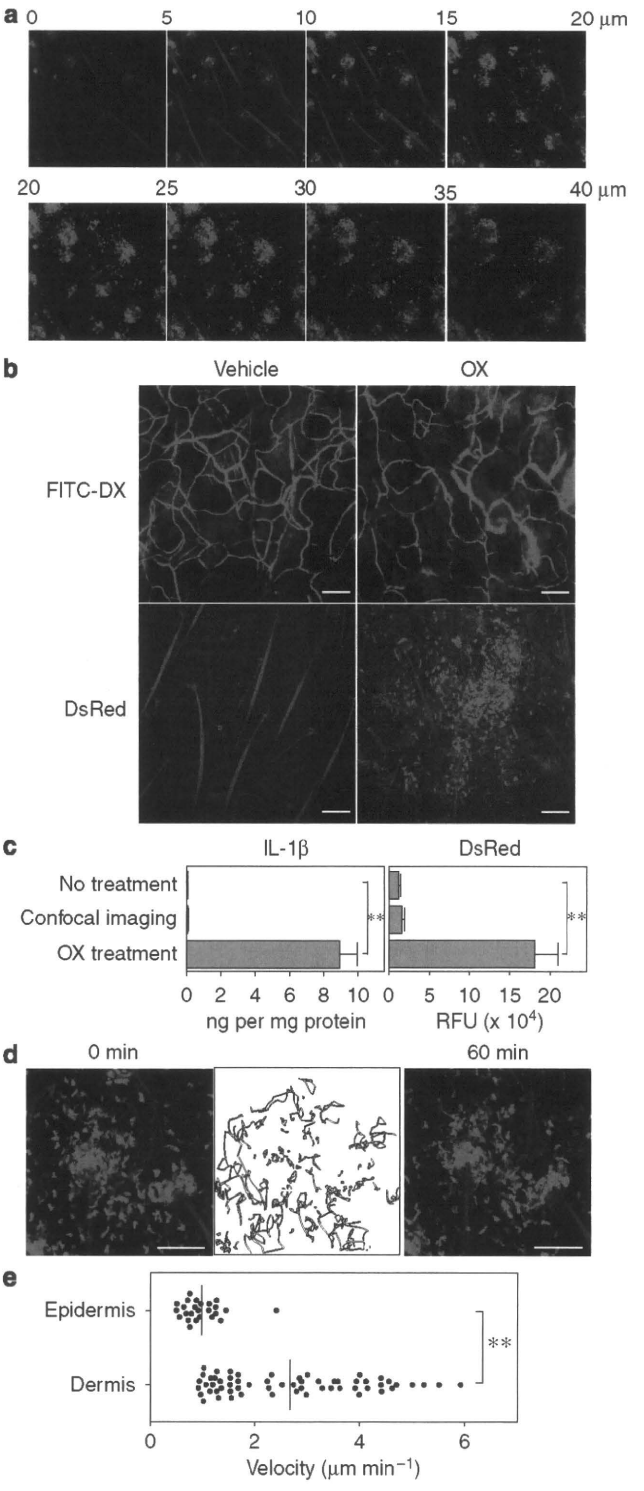

Figure 5. Location and movement of DsRed$^+$ cells emerging in inflammatory skin lesions. (**a**) At 24 hours after OX treatment, pIL1-DsRed transgenic mice were anesthetized and examined under a confocal microscope. Data shown are compiled *x–y* plane images of DsRed$^+$ cells in the indicated 5 μm *z*-axis depth range from the skin surface. Bar = 100 μm. (**b**) At 24 hours after topical application of OX or vehicle alone, FITC-DX was intravenously injected into pIL1-DsRed transgenic mice to visualize blood vessels. The images were recorded 5 minutes after FITC-DX injection. Bar = 100 μm. (**c**) At 24 hours after 30-minute-long confocal imaging sessions or OX treatment, ear skin extracts were examined for IL-1β protein and DsRed signals. Data shown are the means ± SD from three mice per group (**$P<0.01$). (**d**) At 24 hours after OX treatment, pIL1-DsRed transgenic mice were anesthetized to record confocal fluorescence images every 2 minutes for 60 minutes. The images represent the locations of DsRed$^+$ cells at the indicated time points (left and right panels) with migratory paths of individual DsRed$^+$ cells (middle panel). Bar = 100 μm. (**e**) The velocity of each DsRed$^+$ cell was calculated from the above tracking experiments. Velocity values were then compared between the epidermal compartment (up to 18 μm from the skin surface) and the dermal compartment (18–35 μm from the skin surface). Bars indicate mean velocity values (**$P<0.01$).

administration of anesthetics) would deliver pathogenic signals to the imaging site, thereby causing artificial inflammatory responses. To test this possibility, we recorded 3D images in the ear of a pIL1-DsRed transgenic mouse and determined whether such procedures would cause immediate or delayed skin inflammation. In the absence of OX application or other proinflammatory stimuli, very few motile DsRed$^+$ cells were observed at the end of continuous time-lapse imaging up to 60 minutes (data not shown). Moreover, we failed to detect significant IL-1β protein production or DsRed expression even 24 hours after 30-minute imaging sessions (Figure 5c). These observations imply that our confocal imaging protocol enables intravital visualization of IL-1β production under relatively physiological conditions.

To assess motile activities of IL-1β-producing cells, we next recorded 3D images of DsRed$^+$ cells every 2 minutes for 60 minutes. Time-lapse videos generated from these data sets showed that DsRed$^+$ cells constantly displaced the cell bodies via amoeba-like motile behavior (Supplementary Movie S4). By tracking *x*–*y* locations of individual DsRed$^+$ cells, we followed the migratory paths of DsRed$^+$ cells within the 60-minute period (Figure 5d). Interestingly, DsRed$^+$ cells seemed to be more motile in the dermis than in the epidermis (Supplementary Movies S5 and S6). In fact, the mean velocity among DsRed$^+$ cells was significantly higher in the dermal compartment ($2.7 \pm 1.4\,\mu m\,min^{-1}$, $n = 60$) than in the epidermal compartment ($1.0 \pm 0.4\,\mu m\,min^{-1}$, $n = 25$) (Figure 5e). Our intravital time-lapse imaging experiments have demonstrated that myeloid leukocytes, which presumably produce IL-1β, crawl through the extracellular matrix around hair follicles in inflamed skin.

Concluding remarks

In this study, we developed a simple experimental system to directly visualize IL-1β promoter activation in living animals. Abundant production of IL-1β mRNA and protein, as well as robust DsRed expression, became detectable in the skin after topical application of contact sensitizers. Flow cytometric and confocal imaging experiments revealed that DsRed fluorescence signals were mostly associated with CD45$^+$/CD11b$^+$ myeloid leukocytes crawling around hair follicles. Our findings may first seem to be contradictory to the previous report that an MHC class II–positive epidermal cell fraction (i.e., LCs) accounted for a majority of IL-1β mRNA detected by RT-PCR after application of contact sensitizers (Enk and Katz, 1992). It should be stated here that they examined IL-1β mRNA expression only in the epidermal compartment. Moreover, we also observed that some DsRed$^+$ epidermal cells exhibited the characteristic phenotype and morphology of LCs. Thus, it seems reasonable to conclude that LCs represent one, but not the only, IL-1β-producing epidermal cell population in inflamed skin.

Somewhat unexpected was our finding of profound entry of DsRed$^+$/CD11b$^+$/Gr-1^{high} leukocytes into both epidermal and dermal compartments. In this regard, Peters *et al.* (2008), using transgenic mice expressing the enhanced green fluorescence protein gene under the control of the lysozyme M promoter, recently demonstrated a rapid and sustained accumulation of CD11b$^+$/Gr-1^{high} neutrophils (expressing no detectable MHC class II or F4/80) at the bite sites of *Leishmania*-infected sand flies. We now show that DsRed$^+$/CD11b$^+$/Gr-1^{high} leukocytes emerge and crawl around hair follicles in inflamed skin. It remains to be determined whether those leukocytes are derived from progenitors residing in hair follicles, which serve as a reservoir for various stem cell populations (Moore and Lemischka, 2006; Fuchs, 2007), or whether they simply exit the circulation preferentially through hair follicle–associated blood vessels. Nevertheless, this study now provides an important piece of information with regard to leukocyte trafficking to and within inflamed skin.

It is equally important to point out the major weaknesses of our study. First, cells expressing DsRed fluorescence signals do not necessarily represent cells producing biologically active 18 kDa IL-1β protein, because 31 kDa pro-IL-1β protein requires caspase-1-dependent cleavage. In this regard, our approach resembles the recent use of human IL-1β promoter for driving luciferase gene expression (Li *et al.*, 2008). The resulting transgenic mice were then monitored for luciferase expression by intravital bioluminescent imaging in a zymosan-induced arthritis model, an LPS-induced acute peritonitis model, and an OX-induced contact dermatitis model. Although their experimental system enabled real-time monitoring of luciferase activities in affected organs, its spatial resolution was far below the level that we achieved with confocal microscopy. Second, IL-1β mRNA and protein expression was readily detected within 6 hours after OX application, whereas DsRed fluorescent signals became detectable 12–24 hours after the same treatment. This apparent time lag probably represents the time interval required for tetramerization of newly synthesized DsRed molecules. One should be able to overcome this technical limitation by using different fluorescence proteins that emit fluorescence signals in monomeric forms. Likewise, DsRed signals remained at measurable levels even after IL-1β protein became almost undetectable—this discordance in time kinetics, which probably reflects the 24–48 hour difference observed in the half-life between IL-1β and DsRed, represents a limitation of our assay system, especially for studying IL-1β-producing cells in the resolution phase of skin inflammation.

In conclusion, the experimental system developed in this study has allowed us to directly monitor the number, phenotype, location, and movement of IL-1β-producing cells in inflamed skin in living animals with relatively high spatial resolution. Recent advances in confocal microscopy, multiphoton laser scanning microscopy, and green fluorescence protein transgenic and knock-in animals have made it possible to visualize the motile behavior of different leukocyte subsets in lymphoid and epithelial tissues (Germain *et al.*, 2006). Our approach now adds another dimension to such intravital imaging studies by providing key information on cellular function.

MATERIALS AND METHODS

Construction of pIL1-DsRed transgenic mice

A 1.2 kb rabbit β-globin gene containing a noncoding intron/exon was obtained by digesting the pSG-1 expression vector with *Bam*HI

and *Xho*I (Toyonaga *et al.*, 1994; Miyazaki *et al.*, 2001). The fragment was subcloned into the *Bam*HI/*Xho*I site of pBK-CMV (Stratagene, La Jolla, CA) to produce the plasmid pBK-CMV-SG. To generate a red fluorescent protein-expressing vector, a PCR fragment was amplified from pDsRed-Express-DR plasmid (Clontech, Palo Alto, CA) using the primer set 5′-GGGAATTCCGG TCGCCACCATGGCCTC-3′ and 5′-GGAGATCTACACATTGATCC TAGCAGAAG-3′ and was subsequently ligated into a TA-cloning vector, pCR4-TOPO (Invitrogen, Carlsbad, CA), and then subcloned between the *Eco*RI and the *Bgl*II sites of pBK-CMV-SG. The resulting vector, pBK-CMV-SG-Red, carried a CMV immediate early promoter upstream of the β-globin intron/exon-RFP fusion gene. The CMV promoter region was removed by digestion with *Vsp*I and *Nhe*I, followed by blunting of both ends with Klenow fragment and self-ligation. The 4,138-bp *Bam*HI fragment of the murine IL-1β promoter was inserted into the *Bam*HI site to generate the plasmid pBK-SG-IL-1β-Red (Godambe *et al.*, 1995). Plasmid pBK-SG-IL-1β-Red was digested with *Sal*I and *Not*I to clear the vector sequences, and the transgene fragment was purified by Elutip-D (Schleicher and Schuell, Keene, NH). The resulting DNA was microinjected into fertilized eggs of C57BL/6 mice. Transgene expression was determined by genomic PCR for DNA isolated from tail biopsies with specific primers, 5′-TGCTGG TTGTTGTGCTGTCTCATC-3′ and 5′-CACGTACACCTTGGAGCCG TACTG-3′. The screening results were subsequently confirmed at the protein level by testing the expression of DsRed fluorescence signals by peripheral blood mononuclear cells after *in vitro* stimulation with LPS. Transgene-positive mice were bred with WT C57BL/6 mice, and heterozygous offspring were used in this study.

Measurement of IL-1β mRNA and protein expression in skin samples

To measure IL-1β mRNA expression, total RNA was isolated from freshly procured ear skin samples using TRIzol reagent (Invitrogen) and the RNeasy Plus Mini Kit (Qiagen, Valencia, CA). Corresponding cDNA was prepared using the SuperScript III First-Strand System Kit (Invitrogen), and real-time PCR was performed using a LightCycler instrument (Roche Applied Science, Indianapolis, IN) with QuantiTect SYBR Green PCR Master Mix (Qiagen) and specific primers for IL-1β (SA Biosciences, Frederick, MD). The amount of IL-1β mRNA was determined relative to glyceraldehyde-3-phosphate dehydrogenase mRNA using the comparative cycle threshold numbers method. Tissue extracts were prepared from ear skin samples using the T-PER Tissue Protein Extraction Reagent supplemented with Halt Protease Inhibitor Cocktail (Thermo Scientific, Rockford, IN). Protein concentration was determined using the BCA assay kit (Thermo Scientific). IL-1β protein levels were examined using an ELISA kit (R&D Systems, Minneapolis, MN), and DsRed fluorescence intensities were measured using the FLUOstar Omega microplate reader (BMG Labtech, Chicago, IL).

Skin inflammation models

Mice received topical application of 1.25% OX (Sigma-Aldrich, St Louis, MO), 0.5% 2,4-dinitrofluorobenzene (MP Biomedicals, Solon, OH), or 90% lactic acid (Sigma-Aldrich) on their right ears using our standard protocol (Nishibu *et al.*, 2006). The treated ears showed statistically significant ($P<0.01$) swelling compared with the left ears of the same animals painted with vehicle alone. Skin inflammation was also induced mechanically by repeated (10 times) tape stripping (Holzmann *et al.*, 2004).

Measurement of IL-1β release and DsRed expression in BM-DCs

BM-DC cultures were generated from pIL1-DsRed transgenic mice in complete RPMI 1640 supplemented with 10 ng ml^{-1} murine granulocyte-macrophage colony-stimulating factor (Matsushima *et al.*, 2009). BM-DCs were pulsed for 1 hour with 300 ng ml^{-1} LPS, washed extensively, and then cultured for various periods in the absence of added LPS. The cells and culture supernatants were examined for DsRed expression and IL-1β protein, respectively.

Optical imaging of DsRed fluorescence signals

For conventional imaging experiments, freshly procured ear skin specimens were fixed with 2% paraformaldehyde for 30 minutes at room temperature and then examined for DsRed fluorescence signals under an MVX10 MacroView system (Olympus, Melville, NY) or a TCS SP5 confocal microscope (Leica Microsystems, Bannockburn, IL). For intravital imaging experiments, the mice were anesthetized with intraperitoneal injection of an anesthetic cocktail (ketamine, xylaxine, and acepromazine) and placed on an imaging stage to mount the tip of the ear, with the ventral side down, to record images of DsRed$^+$ cells under a TCS SP5 confocal microscope controlled by LAS AF Lite software (Leica Microsystems) as described previously (Nishibu *et al.*, 2006). We typically scanned tissues with *x*, *y*, *z* volumes ($387.5 \times 387.5 \times 60$ or $775 \times 775 \times 80\,\mu m$) at 1 μm *z*-steps to create 3D image sets. *Stratum corneum*–associated autofluorescence signals were used as a marker to define the epidermal compartment, i.e., 20 μm from the outermost surface of the *stratum corneum*. Blood vessels were visualized by intravenous injection of 20 mg ml^{-1} of FITC-DX (70 kDa, Sigma-Aldrich). In time-lapse imaging experiments, 3D images were recorded every 2 minutes for 60 minutes and then analyzed using ImageJ (National Institutes of Health) and Photoshop software (Adobe, San Jose, CA). Tracking of DsRed$^+$ cells in living animals was performed with MetaMorph software (Molecular Devices, Sunnyvale, CA). Construction of the pIL1-DeRed transgenic mouse line and its use in imaging experiments were approved by the institutional review boards at the University of Texas Southwestern Medical Center and the University of Toledo College of Medicine, respectively, and all animal experiments were conducted according to guidelines of the National Institutes of Health.

Flow cytometric analyses

Epidermis was separated from ear skin with 0.5% dispase II (Roche Diagnostics, Indianapolis, IN) for 45 minutes at 37 °C. The epidermis was further treated with 0.3% trypsin (Worthington, Lakewood, NJ) in the presence of 0.1% DNase I (Roche Diagnostics) for 10 minutes at 37 °C to prepare single cell suspension. The dermis was minced and incubated for 1 h at 37 °C with 1,000 U ml^{-1} collagenase XI (Worthington), 1,000 U ml^{-1} hyaluronidase IV (Sigma-Aldrich), and 0.1% DNase I. The obtained single-cell suspensions were pretreated for 15 minutes on ice with 5 μg ml^{-1} anti-CD16/CD32 (2.4G2) mAb, and subsequently stained with fluorescence-conjugated mAb for 30 minutes on ice. In addition to isotype-matched controls, the following mAbs were

used: CD11b (M1/70), CD45 (30-F11), IA-IE (2G9), and Gr-1 (RB6-8C5, all purchased from BD Biosciences, Palo Alto, CA), and F4/80 (BM8; eBioscience, San Diego, CA). After the addition of propidium iodide, samples were analyzed with FACSCalibur (BD Biosciences).

Statistical analyses

Differences in measured variables between the experimental and the control groups were assessed with two-tailed Student's *t*-test. Data from time-course experiments were analyzed by analysis of variance and Dunnett's test. All experiments were repeated more than twice to assess reproducibility.

CONFLICT OF INTEREST

The authors state no conflict of interest.

ACKNOWLEDGMENTS

We thank R. Mohr, C. Krout, and R. Lu for technical assistance of imaging experiments; B. Chojnacki, A. Rupp, and J. Baranski for screening and maintenance of animal colonies; and D. Ammons for secretarial assistance. This work was supported by NIH grants (RO1-AI46755, RO1-AR35068, RO1-AR43777, and RO1-AI43232 to AT).

SUPPLEMENTARY MATERIAL

Supplementary material is linked to the online version of the paper at http://www.nature.com/jid

REFERENCES

Antonopoulos C, Cumberbatch M, Dearman RJ *et al.* (2001) Functional caspase-1 is required for Langerhans cell migration and optimal contact sensitization in mice. *J Immunol* 166:3672–7

Auffray C, Sieweke MH, Geissmann F (2009) Blood monocytes: development, heterogeneity, and relationship with dendritic cells. *Annu Rev Immunol* 27:669–92

Cerretti DP, Kozlosky CJ, Mosley B *et al.* (1992) Molecular cloning of the interleukin-1 beta converting enzyme. *Science* 256:97–100

Coeshott C, Ohnemus C, Pilyavskaya A *et al.* (1999) Converting enzyme-independent release of tumor necrosis factor alpha and IL-1beta from a stimulated human monocytic cell line in the presence of activated neutrophils or purified proteinase 3. *Proc Natl Acad Sci USA* 96:6261–6

Cumberbatch M, Dearman RJ, Kimber I (1997) Langerhans cells require signals from both tumour necrosis factor-alpha and interleukin-1 beta for migration. *Immunology* 92:388–95

Dinarello CA (2009) Immunological and inflammatory functions of the interleukin-1 family. *Annu Rev Immunol* 27:519–50

Enk AH, Angeloni VL, Udey MC *et al.* (1993) An essential role for Langerhans cell-derived IL-1 beta in the initiation of primary immune responses in skin. *J Immunol* 150:3698–704

Enk AH, Katz SI (1992) Early molecular events in the induction phase of contact sensitivity. *Proc Natl Acad Sci USA* 89:1398–402

Fantuzzi G, Ku G, Harding MW *et al.* (1997) Response to local inflammation of IL-1 beta-converting enzyme-deficient mice. *J Immunol* 158:1818–24

Fuchs E (2007) Scratching the surface of skin development. *Nature* 445:834–42

Gabrilovich DI, Nagaraj S (2009) Myeloid-derived suppressor cells as regulators of the immune system. *Nat Rev Immunol* 9:162–74

Germain RN, Miller MJ, Dustin ML *et al.* (2006) Dynamic imaging of the immune system: progress, pitfalls and promise. *Nat Rev Immunol* 6:497–507

Godambe SA, Chaplin DD, Takova T *et al.* (1995) A novel cis-acting element required for lipopolysaccharide-induced transcription of the murine interleukin-1 beta gene. *Mol Cell Biol* 15:112–9

Holzmann S, Tripp CH, Schmuth M *et al.* (2004) A model system using tape stripping for characterization of Langerhans cell-precursors *in vivo*. *J Invest Dermatol* 122:1165–74

Kupper TS (1990) Immune and inflammatory processes in cutaneous tissues. Mechanisms and speculations. *J Clin Invest* 86:1783–9

Kupper TS, Ballard DW, Chua AO *et al.* (1986) Human keratinocytes contain mRNA indistinguishable from monocyte interleukin 1 alpha and beta mRNA. Keratinocyte epidermal cell-derived thymocyte-activating factor is identical to interleukin 1. *J Exp Med* 164:2095–100

Li L, Fei Z, Ren J *et al.* (2008) Functional imaging of interleukin 1 beta expression in inflammatory process using bioluminescence imaging in transgenic mice. *BMC Immunol* 9:49

Luger TA, Stadler BM, Luger BM *et al.* (1982) Murine epidermal cell-derived thymocyte-activating factor resembles murine interleukin 1. *J Immunol* 128:2147–52

Martinon F, Mayor A, Tschopp J (2009) The inflammasomes: guardians of the body. *Annu Rev Immunol* 27:229–65

Matsushima H, Tanaka H, Mizumoto N *et al.* (2009) Identification of crassin acetate as a new immunosuppressant triggering heme oxygenase-1 expression in dendritic cells. *Blood* 114:64–73

Miyazaki T, Ohura T, Kobayashi M *et al.* (2001) Fatal propionic acidemia in mice lacking propionyl-CoA carboxylase and its rescue by postnatal, liver-specific supplementation via a transgene. *J Biol Chem* 276:35995–9

Mizumoto N, Gao J, Matsushima H *et al.* (2005) Discovery of novel immunostimulants by dendritic-cell-based functional screening. *Blood* 106:3082–9

Moore KA, Lemischka IR (2006) Stem cells and their niches. *Science* 311:1880–5

Nakae S, Naruse-Nakajima C, Sudo K *et al.* (2001) IL-1 alpha, but not IL-1 beta, is required for contact-allergen-specific T cell activation during the sensitization phase in contact hypersensitivity. *Int Immunol* 13:1471–8

Nambu A, Nakae S, Iwakura Y (2006) IL-1beta, but not IL-1alpha, is required for antigen-specific T cell activation and the induction of local inflammation in the delayed-type hypersensitivity responses. *Int Immunol* 18:701–12

Nishibu A, Ward BR, Jester JV *et al.* (2006) Behavioral responses of epidermal Langerhans cells *in situ* to local pathological stimuli. *J Invest Dermatol* 126:787–96

O'Neill LA (2008) The interleukin-1 receptor/Toll-like receptor superfamily: 10 years of progress. *Immunol Rev* 226:10–8

Peters NC, Egen JG, Secundino N *et al.* (2008) *In vivo* imaging reveals an essential role for neutrophils in leishmaniasis transmitted by sand flies. *Science* 321:970–4

Shornick LP, De Togni P, Mariathasan S *et al.* (1996) Mice deficient in IL-1beta manifest impaired contact hypersensitivity to trinitrochlorobenzone. *J Exp Med* 183:1427–36

Sugawara S, Uehara A, Nochi T *et al.* (2001) Neutrophil proteinase 3-mediated induction of bioactive IL-18 secretion by human oral epithelial cells. *J Immunol* 167:6568–75

Takashima A, Bergstresser PR (1996) Impact of UVB radiation on the epidermal cytokine network. *Photochem Photobiol* 63:397–400

Thornberry NA, Bull HG, Calaycay JR *et al.* (1992) A novel heterodimeric cysteine protease is required for interleukin-1 beta processing in monocytes. *Nature* 356:768–74

Toyonaga T, Hino O, Sugai S *et al.* (1994) Chronic active hepatitis in transgenic mice expressing interferon-gamma in the liver. *Proc Natl Acad Sci USA* 91:614–8

Watanabe H, Gaide O, Petrilli V *et al.* (2007) Activation of the IL-1beta-processing inflammasome is involved in contact hypersensitivity. *J Invest Dermatol* 127:1956–63

注目される用語の解説

AIM

新井郷子（東京大学大学院医学系研究科疾患生命工学センター分子病態医科学部門講師）
宮崎　徹（東京大学大学院医学系研究科疾患生命工学センター分子病態医科学部門教授）

AIMはマクロファージが産生する分泌蛋白質

AIMは分化成熟したマクロファージが特異的に産生する3つのSRCR（scavenger receptor cystein-rich）ドメインからなる分泌型蛋白質である。1999年に同定し、マクロファージ自身のアポトーシスを抑制する機能をもつことからapoptosis inhibitor of macrophage（AIM）と命名した（ほかにCD5L、Spα、Api6などの呼称がある）[1]。AIMは分泌型蛋白質であるため、そのアポトーシス抑制機構はおそらく受容体を介したものであると考えられるが、Fasや放射線、ステロイド、または細菌感染、細胞ストレスなど、さまざまなタイプのアポトーシス誘導に対し抵抗性を示すことからも[1, 2]、特定のアポトーシス誘導シグナルを阻害するというより、細胞のviabilityを高めているという見方のほうがふさわしいかもしれない。アポトーシス抑制の詳細な分子メカニズムは現在解析中である。

AIMは動脈硬化の病態進行に深く関与する

AIMはマクロファージにおいて核内受容体LXR（liver X receptor）/RXR (retinoid X receptor) ヘテロ二量体の活性化により強く誘導される。LXRは酸化LDLの分解物であるオキシステロールをリガンドとして活性化され、ほかには*ABCA-1*（*ATP-binding cassette, sub-family A, member 1*）や*ApoE*（*apolipoprotein E*）など、細胞外へのコレステロール排出系統にかかわる重要な分子群の遺伝子発現を誘導することが知られている。

高コレステロール血症下では動脈の血管内皮下層における酸化LDL濃度が高まり、掃除屋マクロファージが浸潤して酸化LDLを貪食する。酸化LDLを取り込んだマクロファージは細胞内にコレステロールエステルを溜め込んで泡沫化して膨れ上がり、内皮下層に蓄積していくことで動脈硬化巣形成の礎となるが、そのような細胞は酸化LDLの刺激によりLXRが強く活性化されているために、AIMを非常に強く産生している[3]。そのため、硬化巣マクロファージは、酸化LDLや炎症性サイトカイン類、Fas-Fasリガンド系などの細胞間相互作用、一酸化窒素（NO）などのさまざまなアポトーシス誘導性物質や、局所的な低栄養状態、低酸素状態などの環境悪化に常に曝されているにもかかわらず、アポトーシス抵抗性を示す。このことは硬化巣において泡沫化細胞の蓄積とそれに伴う病巣の炎症反応の持続をもたらし、病態進行の悪化の原因になる。実際に、AIM非存在下では、硬化巣においてマクロファージのアポトーシスの顕著な増加がみられ、さらにそれに

図1　AIMの欠損による動脈硬化の軽減

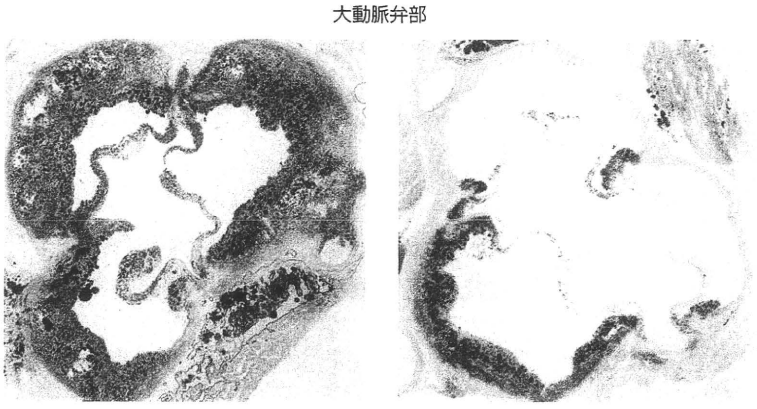

$AIM^{+/+}LDLR^{-/-}$　　$AIM^{-/-}LDLR^{-/-}$

高コレステロール食を12週間与えたマウスに形成された動脈硬化巣

LDLR：LDL受容体　　（文献3より引用）

図2　肥満の進行と脂肪細胞によるAIMの取り込み

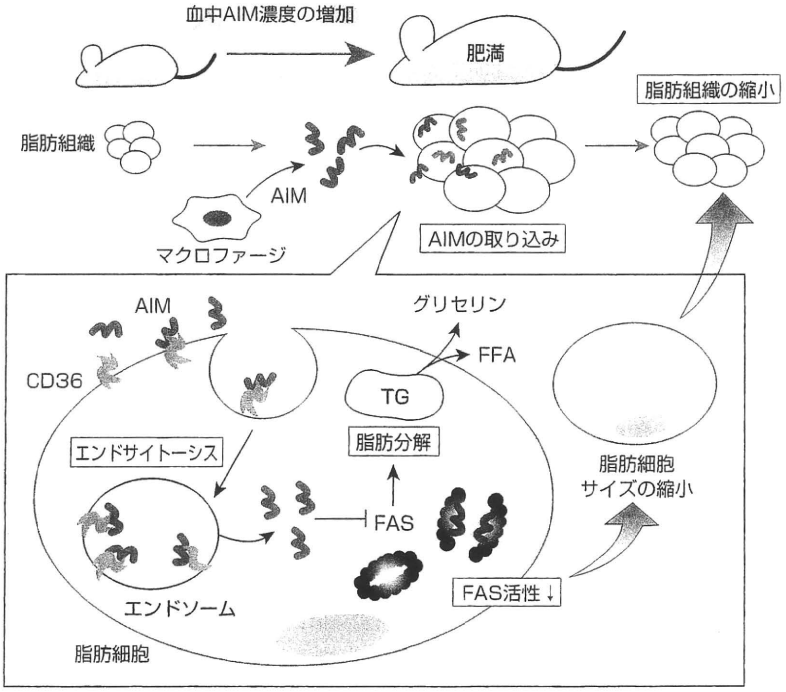

FAS：脂肪酸合成酵素　TG：triglyceride（中性脂肪）　FFA：free fatty acid（遊離脂肪酸）

伴う病巣の炎症反応の軽減により、病態の初期から後期にかけて動脈硬化の著しい軽減が観察されることがAIMを欠損した動脈硬化モデルマウス（*$AIM^{-/-}$ $LDLR^{-/-}$マウス*）を用いて示されている[3]（**図1**）。

最新トピックス：AIMは脂肪細胞によって取り込まれ、脂肪分解を誘導する

上記の知見に加え、最近われわれは脂肪細胞におけるAIMの新たな機能を発見した[4]（**図2**）。分泌型